JCI The Journal of Clinical Investigation

# Reduced vaccine-induced germinal center outputs in inflammatory bowel disease patients treated with anti-TNF biologics

Michelle W. Cheung, … , Anne-Claude Gingras, Tania H. Watts

*J Clin Invest.* 2025. https://doi.org/10.1172/JCI192589.

Clinical Research and Public Health | In-Press Preview | Immunology | Infectious disease

## Graphical abstract

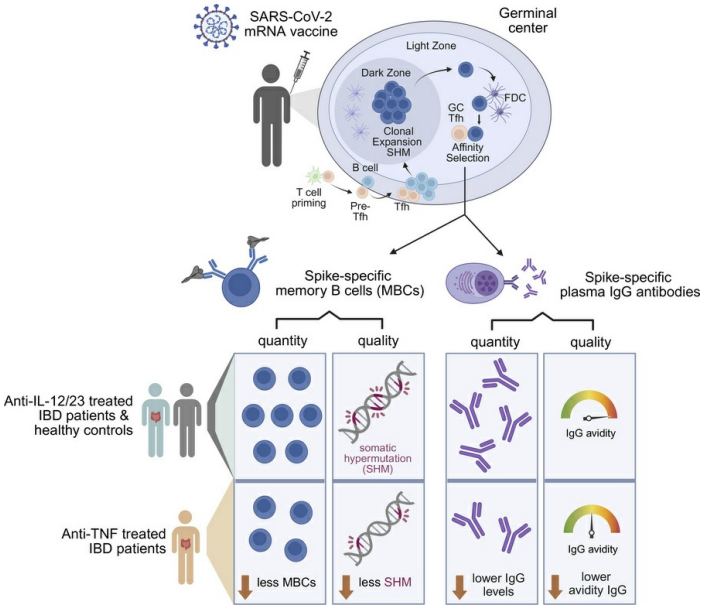

**Title:** Reduced vaccine-induced germinal center outputs in inflammatory bowel disease patients treated with anti-TNF biologics

**Authors:** Michelle W. Cheung,[1] Samantha Xu,[1] Janna R. Shapiro,[1] Freda Qi,[2] Melanie Delgado-Brand,[2] Karen Colwill,[2] Roya M. Dayam,[2] Ying Liu, [3] Jenny D. Lee,[2,4] Joanne M. Stempak,[2,4] James M. Rini,[3,5] Vinod Chandran,[6,7,8,9] Mark S. Silverberg,[2,4,10] Anne-Claude Gingras,[2,3] Tania H. Watts,[1,*]

**Affiliations:**

[1]Department of Immunology, University of Toronto; Toronto, Ontario, Canada.

[2]Lunenfeld-Tanenbaum Research Institute at Mount Sinai Hospital, Sinai Health System; Toronto, Ontario, Canada.

[3]Department of Molecular Genetics, University of Toronto; Toronto, Ontario, Canada.

[4]Zane Cohen Centre for Digestive Diseases, Division of Gastroenterology, Mount Sinai Hospital, Sinai Health System; Toronto, Ontario, Canada.

[5]Department of Biochemistry, University of Toronto; Toronto, Ontario, Canada

[6]Gladman Krembil Psoriatic Arthritis Research Program, Schroeder Arthritis Institute, Krembil Research Institute, University Health Network; Toronto, Ontario, Canada

[7]Division of Rheumatology, Department of Medicine, University of Toronto; Toronto, Ontario, Canada

[8]Department of Laboratory Medicine and Pathobiology, University of Toronto; Toronto, Ontario, Canada

[9]Institute of Medical Science, University of Toronto; Toronto, Ontario, Canada

[10]Division of Gastroenterology, Department of Medicine, University of Toronto; Toronto, Ontario, Canada.

*Corresponding author: Tania H. Watts

Address: 1 King's College Circle, Toronto, Ontario, Canada, M5S 1A8

Telephone: 416-978-4551

Email: tania.watts@utoronto.ca

**Conflict-of-interest Statement:**

A.-C.G. has received research funds from a research contract with Providence Therapeutics Holdings, Inc., for other projects, participated in the COVID-19 Immunity Task Force Immune Science and Testing working party, chaired the Canadian Institutes of Health Research Institute of Genetics Advisory Board, and chairs the Science Advisory Board of the National Research Council of Canada Human Health Therapeutics Board. V.C. has received research grants from AbbVie, Johnson and Johnson, and Eli Lilly and has received honoraria for advisory board member roles from AbbVie, Bristol Myers Squibb, Eli Lilly, Fresenius Kabi, Johnson and Johnson, Novartis, and UCB. His spouse is an employee of AstraZeneca. M.S.S. has received research support, consulting fees, and speaker honoraria from AbbVie, Johnson and Johnson, Takeda, Pfizer, Gilead, and Amgen. All other authors have no financial conflicts of interest.

**Structured Abstract:**

**Background:** Anti-TNF biologics are widely used to treat patients with immune-mediated inflammatory diseases. In mouse models, the complete absence of TNF impairs germinal center (GC) responses. Less is known about the impact of anti-TNF therapy on specific immune responses in humans. Widespread vaccination against SARS-CoV-2 offered an unprecedented opportunity to investigate the effects of biological therapies on responses to specific immunization. Previous work demonstrated that inflammatory bowel disease (IBD) patients treated with anti-TNF biologics exhibit decreased Spike-specific antibody responses compared to IBD patients treated with anti-IL-12/23 or healthy controls, even after four doses of mRNA vaccine.

**Methods:** Here we analyzed humoral responses to SARS-CoV-2 immunization using single-cell RNA-Sequencing and flow cytometry of Spike-specific memory B cells (MBC), as well as avidity measurements of plasma antibodies from IBD patients treated with anti-TNF or anti-IL-12/23 and from healthy controls.

**Results:** We observed decreased somatic hypermutation in the B cell receptors of Spike-specific MBCs and decreased antigen-specific MBC accumulation following SARS-CoV-2 mRNA vaccination in anti-TNF treated IBD patients, compared to IBD patients treated with anti-IL-12/23 or healthy controls. This decreased somatic hypermutation in Spike-specific MBCs in anti-TNF treated patients correlated with decreased and delayed antibody affinity maturation and reduced neutralization activity.

**Conclusion:** These data provide in vivo evidence that anti-TNF, but not anti-IL-12/23, therapy impairs the quantity and quality of antigen-specific GC outputs in humans.

**Funding:** Juan and Stefania Speck (donation) and by Canadian Institutes of Health Research (CIHR)/COVID-Immunity Task Force (CITF) grants VR-1 172711, VS1-175545, GA2-177716, GA1-177703 and CIHR FDN 143301 &143350.

## Main Text:

## Introduction

Immune-mediated inflammatory diseases (IMIDs) comprise a large group of heterogenous, chronic, and disabling conditions that involve one or more organs and share common inflammatory pathways. The estimated prevalence of IMIDs in North America and Europe is 5-7%, and in 2019, the global incidence of IMIDs was approximately 67.5 million cases (1, 2). Anti-cytokine biologics, such as TNF blocking Abs, are among the most widely used therapeutics for the treatment of these conditions (3, 4).

IMID patients have greater susceptibility to viral infections (5, 6). However, few studies have tested the effect of cytokine blockade on a specific immune response in these patients (7). The prioritization of IMID patients for early vaccination against SARS-CoV-2 in Canada provided an opportunity to study in detail how anti-cytokine biologics impact the response to a specific immunization. The IMPACT study (**IM**mune res**P**onse **A**fter **C**OVID-19 vaccination during maintenance **T**herapy in IMIDs) investigated the immune responses to SARS-CoV-2 mRNA vaccination in a cohort of uninfected IMID patients treated with anti-metabolites or anti-cytokine biologics, from pre-vaccination to up to four doses of vaccine (8, 9). While IMID patients overall showed decreased T cell responses after two doses of vaccine compared to healthy controls, these differences were largely eliminated after a third dose (8, 9). However, Ab responses revealed striking differences between treatment groups, such that anti-TNF treated inflammatory bowel disease (IBD) patients had decreased Spike (S)-specific Ab responses even after four doses of vaccine, compared to healthy controls and IBD patients treated with other therapies (8). These findings agree with other studies reporting impaired vaccine induced

humoral responses in IMID patients treated with anti-TNF in the context of SARS-CoV-2 (10-15), influenza (16-18), and hepatitis B vaccines (19).

The mechanism by which anti-TNF Abs impair the humoral response to vaccination in humans remains incompletely understood. TNF is a potent proinflammatory cytokine with pleiotropic effects on the immune system and is critical for the proper organization of germinal centers (GC) within lymphoid organs (20, 21). In GCs, B cells acquire somatic hypermutations (SHM) in their antigen specific B cell receptors (BCRs). These mutated B cells compete for antigen, and those with the highest affinity receptors undergo preferential clonal expansion, leading to affinity maturation of the B cell response (22). This iterative process requires the complex interplay between B cells, T follicular helper cells (Tfh) and follicular dendritic cells (FDCs) (22). Selected GC B cells differentiate into memory B cells (MBCs) and long-lived Ab secreting plasma cells (LLPCs), with the LLPCs emerging later in the GC response and enriched in cells that secrete high affinity Abs (23). Most research on the role of TNF in GCs has been conducted in murine models, where B cell-derived TNF and lymphotoxin beta are required for the development of mature splenic FDC networks (24). TNF-and TNFR1-deficient mice cannot form splenic primary B cell follicles nor organized FDC networks, and upon immunization with T cell-dependent antigens, fail to generate GCs in peripheral lymphoid organs, resulting in impaired IgG responses (20, 21). In humans, treatment of rheumatoid arthritis (RA) patients with the TNFR2 decoy receptor etanercept led to reduced peripheral MBCs frequencies, diminished FDC networks in tonsils, and reduced GC counts and sizes compared to methotrexate-treated RA patients and healthy controls (25). Together, these findings suggest TNF blockade disrupts GCs, in part by affecting FDC networks and the formation and maintenance of GCs. However, the

precise impact of this treatment on GC outputs during a specific immune response in humans remains poorly understood.

The availability of longitudinal human blood samples from SARS-CoV-2 vaccinated yet uninfected IMID patients provides an unprecedented opportunity to investigate the effects of cytokine blockade on a specific immune response. To this end, we isolated SARS-CoV-2 S-specific MBCs from the blood of vaccinated anti-TNF or anti-IL-12/23-treated IBD patients as well as from vaccinated healthy controls. We demonstrate that anti-TNF Ab treated IBD patients exhibit altered GC outputs in response to SARS-CoV-2 mRNA vaccination, characterized by reduced SHM and a lower frequency of S-specific MBCs. These findings correlated with lower levels of S-specific IgG and reduced and delayed affinity maturation of the Ab response. In contrast, the GC outputs of anti-IL-12/23 treated IBD patients were indistinguishable from healthy controls. Our findings are one of the few in-human studies demonstrating the effect of TNF blockade on a specific immune response.

## Results

### Study design and participant characteristics

This study used residual stored PBMC and plasma from the IMPACT study (8, 9). Samples were selected from IMID patients diagnosed with IBD (ulcerative colitis or Crohn's disease) on maintenance treatment with anti-TNF or anti-IL-12/23 biologics. As anti-TNF and anti-IL-12/23 treated IBD patients had broadly similar T cell responses to SARS-CoV-2 vaccination, but differed in their humoral responses, the anti-IL-12/23 treated IBD patients along with healthy donors served as controls to assess the impact of anti-TNF on GC outputs to vaccination (8, 9). The anti-TNF Abs included infliximab, adalimumab, or golimumab, however, only the patients on infliximab were used for single-cell RNA-Seq. The anti-IL-12/23 biologic used was ustekinumab. Except for one patient who received 3mg/day of the corticosteroid Entocort, all patients in this study were treated with a single immunomodulatory drug. The majority (at least 75% at each time point) of the IBD patients were in remission and all were on maintenance treatment throughout the study (Supplementary Tables 1-3). None of the participants used in this analysis had been infected with SARS-CoV-2 at the time of sampling, based on testing seronegative for nucleocapsid protein as well as on self-reporting. Figure 1A shows the vaccination and sample collection schedule for this study. MBCs for single-cell RNA-Seq were isolated from samples taken at 3-4 months after the 2$^{nd}$ and 3$^{rd}$ vaccine doses, to allow time for MBC responses to develop. Table 1 and Supplemental Tables 1-3 provide in-depth demographics and sample sizes for each readout. Ethnicity data were not collected for these patients.

### Altered proportions of S-specific MBC subsets in anti-TNF treated IBD patients

To identify S-specific MBCs for sequencing analysis, we generated S-Streptavidin Phycoerythrin (S-PE) tetramers corresponding to the original Wuhan strain of SARS-CoV-2 used in the vaccine. The specificity of S-PE tetramer binding was validated using PBMCs from pre-vaccination and post-vaccination healthy donors (Supplementary Figure 1). MBCs were defined based on the expression of IgD and CD27, thereby excluding naïve B cells ($IgD^+CD27^-$) (Supplemental Figure 1A). We observed some S-PE tetramer background binding to naïve B cells in both pre- and post-vaccination samples, however, as naïve B cells were excluded from subsequent analysis, this was not a concern. Importantly, there was minimal S-PE tetramer binding to MBCs obtained from pre-vaccination samples and the frequency of $S\text{-}PE^+$ MBCs increased ~10-fold in post-vaccination samples (Supplemental Figure 1B), confirming that the S-PE tetramer binding was specific.

We performed 5' immune profiling via single-cell RNA-Seq and BCR-Seq on S-PE-binding MBCs sorted from the B-cell enriched PBMCs of three healthy controls, five anti-TNF treated IBD patients and four anti-IL-12/23 treated IBD patients (Table 1), using matched samples from 3-4 months post dose two and from 3-4 months post dose three (Figure 1). A total of 1268 cells were analyzed post quality control (824 cells post dose two and 444 cells post dose 3, with cell numbers limited by available samples) (Figure 2A). Cells were clustered based on transcriptional data and visualized by uniform manifold approximation and projection. Initial identification of major cell clusters was based on well-known cell-specific markers - naïve B cells: high *IGHD, IGHM, TCL1A,* and *BACH2* expression and lack of the B cell memory marker *CD27*; memory B cells: high *CD27,* low/absent *IGHD* and *CD38*; NK cells: lack *CD19* and *MS4A1* (CD20) expression but express *GNLY* and *NKG7.* Contaminating naïve B cells and NK cells were excluded from downstream analyses and cells were re-clustered to identify MBC

subsets (Figure 2A). Labeling of individual samples with TotalSeq-C hashtag oligo-tagged Abs enabled the demultiplexing of samples by timepoint (Figure 2B), study group (Figure 2C), and individual (Supplemental Figure 2).

Circulating MBCs in human blood can be broadly divided into two subsets. Classical MBCs (cMBCs) derive from germinal centers, express CD27 and CD21 but lack the expression of CD11c, while atypical MBCs (aMBCs) also referred to as double negative (DN) 2 B cells or age-associated B cells, lack CD2*1* and CD27 and express CD11c (26, 27). Marginal zone (MZ) B cells are innate-like B cells that predominantly reside in the splenic MZ, but can also be found in lymph nodes and blood and are largely unswitched, IgM expressing cells (28). In our analyses of S-specific MBCs, we identified three clusters with distinct surface marker and transcriptomic profiles: cMBCs (cluster 1; C1), MZ – like B cells (cluster 2; C2), and aMBCs (cluster 3; C3) (Figure 2D, Supplemental Figure 3). Classical MBCs were identified as $CD27^{+}$ $IgD^{-}$ and were predominantly class-switched, expressing the four *IGHG* subtypes (Figure 2D, Supplemental Figure 3A). Differential gene expression analyses revealed robust expression of *TOX, HOPX,* and *COCH* in cMBCs (Figure 2D, Supplemental Figure 3B), as previously reported (29). Classical MBCs also showed increased *IL-4R, IL-13RA1*, *FCER2* (encoding CD23), and *HLA-DMB,* consistent with increased T cell-derived IL-4 responsiveness and a GC-origin of cMBCs (Supplemental Figure 3B) (30). Cluster 2, which we defined as "MZ-like B cells," contained the greatest proportion of unswitched cells expressing *IGHM* and a lower proportion of cells expressing switched isotype genes (Figure 2D, Supplemental Figure 3A). Furthermore, we observed higher levels of genes associated with the MZ B cell phenotype: *CD24, PLD4*, *MZB1, CD1c*, *FCGR2B*, *TNFRSF13B*, and *GPR183* (EBI2) (Figure 2D, Supplemental Figure 3B) (31-35). *AKT3* and *PTPRJ* (CD148) were upregulated in the MZ-like B cluster (Supplemental Figure

3B), also consistent with the literature (36, 37). Finally, we detected a small population of MBCs lacking CD27 and expressing genes associated with an atypical phenotype such as *ITGAX*, encoding surface protein CD11c, *TBX21*, *TOX*, *SOX5,* Fc-receptor-like genes *FCRLA, FCRL3* and *FCRL5, FGR,* inhibitory receptor *CD72*, and high *CD19* and *CD20* expression (Figure 2D, Supplemental Figure 3, A-B) (38).

To identify whether the transcriptome of S-specific cMBCs and MZ-like B cells differed between study groups, we conducted pairwise differential gene expression analyses between study groups (Supplemental Figure 4). Atypical MBCs were excluded from the analyses given their low cell count. Overall, few transcripts were different between groups. The increased Y chromosome-specific transcripts (*DDX3Y, KDM5D*, *RPS4Y1, TXLNGY, UTY, UPS9Y)* in the anti-TNF treated IBD study group compared to the anti-IL-12/23 treated IBD and healthy control groups likely reflects differences in the male:female ratio in the study groups analyzed (Table 1). We also observed increased MHC class II gene expression in the cMBCs (*HLA-DQA2*, *HLA-DRB6*) (Supplemental Figure 4A) and MZ-like B cells (*HLA-DQA2*, *HLA-DRB5*) (Supplemental Figure 4B) of IBD patients (anti-IL-12/23 or anti-TNF treated) compared to healthy controls. However, we did not observe an increased overall MHC class II expression on total and S-specific cMBCs and MZ-like B cells at the protein level (Supplementary Figure 4, C-D). *RPS26* expression was increased in IBD patients compared to healthy controls. RPS26 has been positively correlated with anemia, which is a common complication in IBD patients, and identified as a differentially expressed gene marker of IBD (39, 40).

To assess quantitative differences in each cluster between healthy controls and treated IBD patients, we calculated the percentage of S-specific MBCs in each of the three MBC subsets, normalized to each individual (Figure 2E). For the anti-IL-12/23 treated IBD and

healthy control patients, most S-specific MBCs were classified as cMBCs, followed by MZ-like B cells and a small fraction of aMBCs (Figure 2E). Atypical MBCs were not detected in healthy controls post dose three, likely due to the low overall counts of S-specific aMBCs isolated rather than a biological effect (Figure 2E). Anti-TNF treated patients tended to have similar or higher percentages of S-specific MZ-like B cells compared to cMBCs (Figure 2E). The anti-TNF treated group had significantly higher proportions of S-specific MZ-like B cells and aMBCs, and lower proportions of cMBCs post dose two and three, compared to anti-IL12/23 treated IBD patients and healthy controls (Figure 2F), based on pairwise permutation tests with bootstrapping using the scProportionTest library in R (41).

**Anti-TNF treated IBD patients have reduced frequencies of S-specific cMBC**

To validate the differences in MBC subsets in the anti-TNF treated patients observed in the RNA-Seq data, we assessed the phenotype of total peripheral blood B cells and S-specific MBCs in the three study groups using flow cytometry (Figure 3, Supplemental Figure 5). These samples were from different individuals than those used for sequencing, thereby serving as a validation cohort (Supplemental Table 1). MBCs in PBMCs collected pre-vaccination and 3-4 months post dose two were subtyped based on surface markers and Ig isotype as either MZ-like B cells ($CD27^+IgD^+$), cMBCs ($CD27^+IgD^-$), or double negative (DN) B cells ($CD27^-IgD^-$). DN B cell subsets were further defined as DN1 ($CD21^+CD11c^-$), DN2 ($CD21^-CD11c^+$) $CD11c^+$ aMBCs, or DN3 ($CD21^-CD11c^-$) (Supplemental Figure 5A) (42). Compared to cMBCs, MZ-like B cells lacked CD23 expression and highly expressed CD21, IgM and CD1c, while $CD11c^+$ aMBCs lacked the expression of CD21 and CD27 and had high levels of CD20 and MHC class II (pan-HLA-DR/DP/DQ) (Supplemental Figure 5B), as previously reported (43, 44).

There were no significant differences in the frequencies of DN B cells, cMBCs, MZ-like B cells or naïve B cells among total peripheral blood B cells between study groups pre-vaccination or post dose 2 (Supplemental Figure 5C). However, healthy controls exhibited higher frequencies of DN1 B cells and lower frequencies of DN3 B cells compared to anti-TNF treated IBD subjects (Supplemental Figure 5D). There was also no difference in the percentage of unswitched $IgM^+$ cMBCs or switched $IgG^+$ or $IgG^-IgM^-$ cMBCs between study groups (Supplemental Figure 5E).

We used S-PE tetramers to determine the frequencies of S-specific MBCs within each subset of MBC at pre-vaccination and 3-4 months post dose two (Figure 3, A-C). Pre-vaccination, there were minimal S-specific aMBCs and cMBCs as expected, however there was a small population of S-specific MZ-B cells (Figure 3B). Significant increases in the percentage of S-specific MBCs relative to total B cells within each MBC subset were observed post dose two (Figure 3B). Strikingly, after two vaccine doses, anti-TNF treated IBD patients demonstrated significantly lower frequencies of S-specific cMBCs compared to anti-IL-12/23 treated IBD patients and lower frequencies of S-specific DN2 $CD11c^+$ aMBCs and cMBCs compared to healthy controls (Figure 3, B-C). There were no differences in the frequencies of S-specific MZ-like B cells between groups (Figure 3, B-C). These data demonstrate a decreased frequency of antigen-specific MBCs in anti-TNF treated patients; in contrast, the relative frequencies of B cell subpopulations among total peripheral blood B cells were similar in all three study groups. Thus, anti-TNF therapy impairs the induction of S-specific cMBCs following vaccination, consistent with their decreased proportion as evidenced by the RNA-Seq data.

**Biased BCR $V_H$ and $V_L$ gene usage in S-specific MBCs**

Next, we analyzed BCR sequences of S-specific MBCs post vaccine doses two and three across the three study groups. Clones were identified as cells sharing common heavy chain V and J genes and harboring the same complementarity determining region (CDR) 3 length. A total of 1100 BCRs, combined from all individuals and timepoints, were analyzed (Figure 4). We quantified clonal diversity (D) over a range of diversity orders of S-specific MBCs from the three study groups (Figure 4A) (45). Across all metrics of diversity, high diversity was observed for anti-IL-12/23- or anti-TNF treated IBD patients and healthy controls. We also observed high degrees of diversity when cells were stratified by individual (Figure 4B). Some clonal expansion was observed after a third dose of vaccine in healthy controls and anti-IL-12/23 treated IBD patients, although not in the anti-TNF treated study group (Figure 4B).

To examine the repertoire of S-specific MBCs, we compared heavy ($V_H$) and light ($V_L$) chain variable gene usage across study groups (Figure 4C). Gene usage frequencies in each study group were compared to the CoV-AbDab public database of published or patented Abs reported to bind coronaviruses, which we specifically filtered for database entries that were reported to bind SARS-CoV-2 S (Figure 4C) (46). *VH3* family genes were particularly abundant, followed by *VH1* and *VH4* families (Figure 4C). The most abundant $V_H$ genes in all three study groups mirrored the top gene usages in the CoV-AbDab database (*IGHV1-69* and *IGHV3-30*). An enriched usage of *IGKV1-39*, *IGKV3-11*, *IGKV3-20*, and *IGLV2-14* were observed in the three study groups and in the CoV-AbDab database (Figure 4C). Visualization of paired $V_H$ and $V_L$ gene usage of S-specific MBCs is shown in Supplemental Figure 6. Of the 48 gene pairs detected as shared by the three study groups, an enrichment in the usage of *IGHV1-69D/IGKV3-11* was observed based on the count of S-specific MBCs detected (Supplemental Figure 7). Overall, $V_H$ and $V_L$ repertoire analyses revealed high diversity in each study group, as well as conserved V

gene usages and V gene pairs across study groups, suggesting that the biological treatments (anti-IL-12/23 and anti-TNF Abs) had little or no impact on Ab diversity.

**Altered proportions of class switched S-specific MBCs in anti-TNF treated IBD patients**

The BCR-seq data revealed that the cMBCs were largely class-switched, expressing *IGHG1-4* or *IGHA1,* with *IGHG1* expression most predominant (Figure 5A). In contrast, ~75% of MZ-like B cells expressed *IGHM* whereas ~25% were class-switched. Atypical MBCs were heterogenous but predominantly class-switched, albeit harboring a greater fraction of non-switched *IGHM* expressing cells than cMBCs (Figure 5A). When considering total S-specific MBCs (subsets pooled), anti-TNF treated IBD patients exhibited a lower proportion of MBCs expressing *IGHG1-4* class-switched BCRs, and concomitantly, a greater proportion of BCRs expressing *IGHM* (Figure 5B). As most cMBCs expressed class-switched BCRs in all three study groups (Figure 5C), the lower proportion of switched MBCs in anti-TNF treated IBD patients overall may reflect the decreased frequency of cMBCs (Figure 2C), rather than a decrease in class-switch.

**Decreased S-specific IgG, but similar S-specific IgM levels, in plasma from anti-TNF treated IBD patients**

To investigate more directly the potential impact of anti-TNF on Ab class-switch, we conducted ELISA assays for S-specific IgG and IgM from the three study groups. The results showed that across four vaccine doses, anti-TNF treated IBD patients had significantly reduced S-specific IgG levels, compared to anti-IL-12/23 treated IBD patients and healthy controls (Figure 5D), consistent with our earlier studies (8, 9). In contrast, levels of S-specific IgM were

similar across the three groups. These data show a reduced output of IgG without a proportional increase in IgM, consistent with reduced LLPC output from the GC, rather than a reduction in Ab class-switch.

**Reduced somatic hypermutation in anti-TNF treated IBD patients**

SHM in Ig variable (V) regions is important in the affinity maturation of Ab responses. Therefore, we compared the frequency of SHM in the V regions of heavy ($V_H$) and light ($V_L$) chains of MBCs derived from healthy controls and anti-cytokine treated IBD patients (Figure 6, Supplemental Figure 8). Overall, cMBCs had the greatest frequencies of $V_H$ and $V_L$ mutations, followed by MZ-like B cells and aMBCs, irrespective of whether two or three doses of vaccine were received (Supplemental Figure 8, A-B). Stratification by study group revealed that anti-TNF treated IBD patients had significantly lower frequencies of $V_H$ mutations in total S-specific MBCs compared to both the anti-IL-12/23 treated IBD patients and healthy controls after the third dose of vaccine, with differences between the anti-IL-12/23 and anti-TNF groups also observed after dose two (Figure 6A). The greatest differences in the frequencies of $V_H$ mutations were observed in the cMBCs, with anti-TNF treated IBD patients' cMBCs exhibiting lower mutation frequencies compared to the other two groups post dose two (Figure 6B). Similar results were seen with $V_L$ mutations, whereby anti-TNF treated IBD patients had a lower frequency of mutations compared to anti-IL-12/23 treated IBD patients and healthy controls (Supplemental Figure 8C).

When SHMs in the CDRs (CDR1-3) increase the affinity of the BCR for antigen, those cells are selected for clonal expansion in the GC, resulting in affinity maturation. In contrast, mutations in structurally important positions in the framework regions are selected against (47).

Therefore, we further characterized the frequency of mutations by location and the type of mutation (replacement or silent). The bulk of SHMs in the MBC BCRs in all study groups were replacement mutations concentrated in CDR1-3, with fewer SHM in the framework regions (Supplemental Figure 8D). Anti-TNF treated IBD patients exhibit lower frequencies of replacement $V_H$ mutations in CDR1-3 compared to anti-IL-12/23 treated IBD patients post dose two and three, and lower mutation frequencies in CDR1 compared to healthy controls post dose three (Figure 6C). Taken together, the data show that the BCRs of S-specific MBCs from anti-TNF treated patients exhibit less SHM, with the majority being replacement mutations, suggesting that the B cells in the anti-TNF group have undergone less efficient affinity maturation in the GC.

**Anti-TNF treated IBD patients have lower avidity anti-S IgG across four vaccine doses**

We next asked if the reduced SHM frequency in the BCRs of S-specific MBCs from anti-TNF treated IBD patients post vaccination was associated with a lower avidity plasma Ab response. We used a modified ELISA in which increasing concentrations of the chaotropic agent ammonium thiocyanate were added prior to the addition of the secondary Ab, to assess the strength of the Ab-antigen interaction (48-51). We analyzed the avidity of Ab binding to Wuhan S (Figure 7), with avidity reported as a total relative avidity index (TRAI), as defined in the methods. At the time of sample collection, healthy controls were not prioritized for a fourth dose of vaccine, hence data are not available beyond the third dose for the healthy controls. Likewise, we did not have sufficient participants in the anti-TNF treated IBD group to evaluate avidity at the 3-4 months post dose four timepoint. In all participants, anti-S IgG avidity significantly increased with each successive dose of vaccine, plateauing after three vaccine doses in anti-IL-

12/23 treated and anti-TNF treated IBD patients (Figure 7A, Supplemental Table 4). The second dose of vaccine induced the most robust increase in the avidity of S-binding IgG in healthy controls and anti-IL-12/23 treated IBD patients, whereas anti-TNF treated IBD patients exhibited the greatest boost in the avidity of S-binding IgG after the third dose (Figure 7A). Furthermore, the boost in Ig avidity post dose three in anti-TNF patients was decreased compared to the boost in avidity post dose two in healthy controls and anti-IL-12/23 treated IBD patients, highlighting delayed and decreased affinity maturation (Figure 7A). Strikingly, across one to four doses of vaccine, anti-TNF treated IBD patients showed significantly lower avidity IgG binding to S compared to healthy controls and IL-12/23 treated IBD patients (Figure 7A), consistent with the BCR-Seq data presented above. This reduced avidity in the anti-TNF treated group was independent of the type of anti-TNF Ab used (infliximab or adalimumab; Supplemental Figure 9).

We next performed several sensitivity analyses to further interrogate the Ab avidity. First, given that avidity maturation develops over time, we evaluated whether the time between vaccination and sampling impacted the avidity readouts. Within each timepoint analyzed, the time of sampling relative to vaccination was indistinguishable between study groups (Supplemental Figure 10A). Moreover, regression analyses indicated that the time between vaccination and sampling was not predictive of the avidity of anti-S IgG, likely reflecting the relatively homogeneous sampling times (Supplemental Figure 10B). We also assessed the impact of the time between anti-IL-12/23 or anti-TNF infusion and blood sampling on Ab avidity. For samples in which we had the patient self-reported date of most recent infusion, regression analyses revealed no impact of infusion timing on the avidity measurements (Supplemental Figure 11).

We also observed that the avidity of anti-S IgG measured here was positively associated with our previously reported neutralization capacity for Wuhan SARS-CoV-2-post dose two and post dose three (Figure 7B). Thus, higher avidity IgG predicts greater neutralization capacity against the Wuhan strain of virus.

Given that MBCs and LLPCs (a source of plasma IgG) are both cellular outputs of GCs, we examined whether the SHM analyses from BCR-Seq predicted plasma IgG avidity by linear regression analyses. Indeed, we observed that the frequency of $V_H$ mutations in total S-specific MBCs (cMBCs, MZ-like B cells, and aMBCs pooled) or S-specific cMBCs alone predicts the avidity of plasma S-specific IgG (Figure 7C). Anti-TNF treated IBD patients had less SHM and this predicted a lower avidity response (Figure 7C).

By analysis of the proportion of Abs that resist successive washes with ammonium thiocyanate, the responses can be binned into binding categories, ranging from very low to high avidity, for each study group (Figure 7D). After one dose of vaccine, we observed that the majority of antigen-specific IgGs were of very low or low avidity in all groups (Figure 7D). With successive doses of vaccine, the percentage of very low and low avidity IgG decreased, with a corresponding increase in the percentage of medium and high avidity IgG, indicative of affinity maturation (Figure 7D). Compared to healthy controls, after two and three vaccine doses, anti-TNF treated IBD patients had a significantly higher percentage of medium avidity S-specific IgG and a correspondingly lower percentage of high avidity IgG (Figure 7, D-E). Overall, these data demonstrate that vaccine induced responses in anti-TNF treated patients show reduced and delayed affinity maturation relative to anti-IL-12/23 treated patients or healthy controls.

## Discussion

We and others have previously reported a decreased magnitude and persistence of Ab responses to SARS-CoV-2 mRNA vaccination in IMID patients treated with anti-TNF (8-11). In our previous study, decreased S-specific Ab levels were observed only in anti-TNF treated IBD patients, whereas S-specific Ab responses of rheumatic disease patients were not affected, potentially due to the lower doses of anti-TNF agents used (8). Here we performed an in-depth investigation of the effect of anti-TNF on GC outputs in IBD patients in response to vaccination. We observed reduced S-specific BCR SHM, as well as decreased and delayed affinity maturation in anti-TNF treated IBD patients compared to anti-IL-12/23 treated patients or healthy controls. We also observed a decreased frequency of vaccine induced cMBCs. As anti-IL-12/23 treated IBD patients were largely indistinguishable from healthy controls in their Ab responses and MBC phenotypes but have the same age distribution and disease state as the anti-TNF treated patients, with the majority in remission at the time of the study, they serve as an ideal control to assess the effect of anti-TNF treatment, independent of any effects of disease. Together, these data support the conclusion that anti-TNF patients have reduced and delayed affinity maturation post vaccination, consistent with impairment of the GC reaction.

Based on single-cell RNA-Seq, we found that a larger fraction of S-specific MBCs derived from anti-TNF treated IBD patients were aMBCs and MZ-like B cells, whereas cMBCs were the most frequent population in healthy controls and anti-IL-12/23 treated patients. This is likely due to a decrease in cMBC output from the GC, rather than an expansion of extrafollicular responses based on our additional immunophenotyping analysis. Flow cytometric analysis of PBMC showed a reduction in the frequency of antigen-specific aMBCs and cMBCs relative to

total populations of these subsets, whereas the S-reactive B cell frequencies among the MZ-like B cell subset did not change between groups.

In contrast to the impact of anti-TNF on vaccine induced S-binding MBCs, immunophenotyping of total B cell subsets (DN, cMBCs, MZ-like B cells, and naïve B cells) revealed no major differences in MBC subsets between the study groups. The impact of anti-TNF on a specific vaccine induced response, but lack of detectable impact on overall MBC populations, may reflect that much of the MBC repertoire is established during childhood and fine-tuned with subsequent exposures (52). Meanwhile, the peak ages of diagnosis for Crohn's disease and ulcerative colitis are 20-30 years and 30-40 years, respectively (53), in line with the median age of diagnosis in our IBD cohort. This suggests that immune responses to vaccination prior to anti-TNF treatment may be intact, while responses to vaccinations delivered while on anti-TNF treatment are likely to be impaired in this group. This likely extends to other antigens, as impaired humoral responses in anti-TNF treated IBD patients have also been demonstrated in the context of influenza vaccination. IBD patients treated with infliximab (anti-TNF) had lower levels of Abs specific for influenza A/H3N2 or A/H1N1 compared to healthy controls, whereas IBD patients treated with ustekinumab (anti-IL-12/23) had similar responses to influenza vaccination as healthy controls (17), similar to our findings with SARS-CoV-2 vaccines.

Although evidence from mouse knockout studies and limited human studies suggested that TNF blockade would impair the GC reaction (20, 21, 25), it was not predictable how substantially anti-TNF maintenance therapy, rather than complete knockout, would impact affinity maturation. Notably, we observed significantly less SHM in the $V_H$ and $V_L$ regions of S-specific MBCs in anti-TNF treated patients, characterized by fewer replacement mutations in CDR1-3. Correspondingly, across four vaccine doses, S binding plasma IgG Abs from anti-TNF

474 treated patients were of lower overall avidity, with a lower proportion of high affinity Abs
475 compared to anti-IL-12/23 treated patients or healthy controls. We also found that the level of
476 SHM in MBC BCRs predicted both the avidity and neutralization activity of plasma Abs. While
477 SHM measurements were derived from MBCs and avidity was assessed from LLPC-derived
478 IgG, the positive association between these measurements likely reflects that both measurements
479 are reading out the quality of the GC response. Together, these data support the conclusion that
480 anti-TNF patients have reduced and delayed affinity maturation post vaccination, consistent with
481 impairment of the GC reaction.

482 A prior study of vaccinated nursing home residents and health care workers reported that
483 the affinity of S-specific IgG Abs increased after the third dose of SARS-CoV-2 mRNA vaccine,
484 with no further increase after the fourth dose (54). Similarly, our assessment of anti-TNF and
485 anti-IL-12/23 treated IBD patients showed that S-specific Ab avidity plateaued after three
486 vaccine doses, albeit the anti-TNF group did not reach the same level of avidity as the anti-IL-
487 12/23 treated group.

488 Another study of SARS-CoV-2 vaccinated and treated IBD patients reported a defect in
489 the affinity maturation of the Ab response of IBD patients after two doses of vaccine, based on
490 decreased S1-RBD tetramer binding to $IgG^+$ MBCs (55). The study reported that the defect in
491 affinity maturation was corrected after a third dose of vaccine; however, the study did not
492 segregate the post third dose results of the IBD group by treatment type or compare the IBD
493 group to healthy controls that received a third dose. In contrast, our study showed that anti-S Abs
494 from anti-TNF treated subjects were of lower overall avidity than Abs from patients treated with
495 anti-IL-12/23, with a notably reduced proportion of high avidity Abs, even after four doses of
496 vaccine. Our study used an established ELISA-based avidity assay (56) incorporating step wise

497 increases in ammonium thiocyanate concentration, enabling the detection of a broad range of Ab
498 avidities, and this may have increased the sensitivity of our assay over a flow cytometry-based
499 tetramer approach.

500 Although S-specific IgG responses were reduced in the anti-TNF group, S-specific IgM
501 was not significantly different between groups. If CSR was substantially impaired, one would
502 have expected increased IgM responses. CSR has been shown to take place largely before entry
503 of B cells into the GC and before the onset of somatic hypermutation (57). Furthermore, in TNF
504 knockout mice, CSR still occurs in the absence of primary B cell follicles or GC, although T-
505 dependent IgG responses were impaired (20). Therefore, the apparent increase in the proportion
506 of S-specific $IgM^+$ MBCs in the anti-TNF group likely reflects the lower frequencies of $IgG^+$
507 cMBCs due to decreased GC outputs, rather than an increase of $IgM^+$ MBCs because of
508 incomplete CSR.

509 We detected a range of frequencies of SHM in the BCRs of MBC, from unmutated to
510 highly mutated clones, indicating that sorting S-PE tetramer binding MBCs prior to sequencing
511 did not selectively enrich for only high affinity clones. Thus, despite the small number of
512 memory B cells analyzed, we believe that we have analyzed a relatively representative
513 repertoire. The diversity of S-specific MBCs did not appear to be reduced in anti-cytokine treated
514 IBD patients compared to healthy controls, thus we did not observe selective expansion of
515 specific, high avidity clonotypes. Polyclonal repertoires of high diversity are expected given the
516 stochastic nature of V, D and J gene recombination during B cell development and the large
517 number of clonotypes we detected from BCR-Seq. However, our study was limited by the small
518 number of BCRs analyzed.

519 Analysis of BCR repertoire revealed high and similar diversity amongst healthy controls
520 and treated IBD patients; thus, anti-cytokine Abs do not appear to impact the repertoire of S-
521 specific MBCs. We observed similar $V_H$ and $V_L$ biased gene usage across study groups as well as
522 agreement with the CoV-AbDab database and published reports with respect to highly
523 represented $V_H$ genes for S or RBD specificities in convalescent or vaccinated individuals (60-
524 63). We also observed public Ab responses in the light chains; *IGKV1-33* and *IGKV1-19* have
525 been reported to be the most used among RBD specific Abs, while *IGKV3-20* and *IGKV3-11* are
526 the most used among S2 Abs (64). We detected 48 paired heavy and light chain variable genes
527 shared between anti-cytokine treated IBD patients and healthy controls and these pairs had been
528 previously reported in a large-scale systematic survey of Ab responses to SARS-CoV-2 (64),
529 consistent with antigen-driven selection. Thus, the overall biased and similar gene usage of S-
530 specific BCRs across our study groups and other studies further supports the convergent
531 evolution of SARS-CoV-2 vaccine induced B cell responses.
532 Limitations of our study include the small number of individuals in each study group and
533 the limited number of cells analyzed in the RNA-Seq data due to constraints on availability of
534 matched patient samples across timepoints from the original IMPACT study and the low
535 frequency of circulating MBCs. Although the anti-TNF- and anti-IL-12/23-treated IBD study
536 groups were heterogenous in terms of type of infusion medication, dosage, and frequency of
537 infusion, the heterogeneity in the type of medication was eliminated in our RNA-Seq analyses by
538 assessing only infliximab-treated patients in the anti-TNF treated group or ustekinumab-treated
539 patients in the anti-IL-12/23 treated group. Moreover, in our assessments of plasma IgG avidity,
540 we were powered to stratify anti-TNF treated IBD patients based on the type of Ab infusion
541 medication (infliximab or adalimumab) and saw no differences between groups. Another

limitation of our study is the focus on memory B cells derived from peripheral blood rather than cells derived from draining lymph nodes, precluding analysis of GC B cells from secondary lymphoid tissues (58). The effects of sampling location are expected to be minimal, however, as clonal overlap between circulating and secondary lymphoid populations has been reported post vaccination (59). As such, our interpretation on the GC reaction is limited to analysis of GC outputs rather than on GC structure.

In sum, our study presents an in-depth analysis of the humoral immune response to SARS-CoV-2 mRNA vaccination in IBD patients treated with anti-TNF or anti-IL-12/23 compared to healthy controls. Our findings suggest that maintenance treatment of IBD patients with anti-TNF Abs, but not anti-IL-12/23, impairs and delays affinity maturation of a vaccine induced Ab response, leading to reduced quantity and quality of GC outputs. These data suggest that patients on anti-TNF maintenance therapy may require additional vaccine boosters to compensate for a delayed and impaired affinity maturation response.

## Methods:

### Study design

This study used residual stored samples from the IMPACT prospective observational cohort, which investigated the **IM**mune res**P**onse **A**fter **C**OVID-19 vaccination during maintenance **T**herapy in a cohort of patients with IMIDs (8, 9). Plasma and PMBCs were isolated from healthy controls and patients with IMIDs at up to eight timepoints spanning pre and post one to four doses of SARS-CoV-2 mRNA vaccine (BNT162b2 Pfizer-BioNTech or mRNA-1273 Moderna) (Figure 1A) (8, 9). Here we used samples from IBD patients treated with anti-IL-12/23 or anti-TNF biologics, and healthy controls. Participants were selected based on similar demographics (age, sex, BMI, disease state) and the availability of samples from the timepoints of interest. All participants were uninfected.

### Sex as a biological variable

All study groups contained male and female participants. When powered to stratify by sex, we did not observe sex differences to be a significant predictor of anti-S Ab levels or avidity. Sex was controlled for in regression models.

### Generation of S-Streptavidin Phycoerythrin (S-PE) tetramers

The expression, purification and biotinylation of the Wuhan SARS-CoV-2 S ectodomain was performed as previously described (65). The full description of the construct is provided in the Supplemental Methods. Of note, the construct contained specific changes to stabilize the prefusion conformation. Streptavidin R-Phycoerythrin conjugate (SA-PE) (premium grade, Invitrogen, S21388) was used to make the S-SA-PE complexes. Biotinylated-S in PBS was

mixed with SA-PE at molar ratio of 8:1 to 6:1 (S:SA-PE) for 2 hours at room temperature, and the SA-PE-S complex was purified by gel filtration (Superose 6 Increase column, Cytiva). Visualization of the complex by negative stain electron microscopy revealed the complex contained two trimeric S proteins per SA-PE complex. The complex was stored in PBS with protease inhibitor (Complete mini protease inhibitor-EDTA free, Roche-11836170001) at 4°C. The S-SA-PE tetramers are referred to as "S-PE" tetramers in the manuscript and figures.

**Single-cell RNA-Seq**

*Sample preparation.* Samples taken at 3-4 months post vaccine dose two and three were used for scRNA-seq and included three healthy controls, five anti-TNF treated IBD patients, and four anti-IL-12/23 treated IBD patients (Table 1) with matching between time points for all but one subject. B cells were isolated from cryopreserved PBMCs (Militenyi Pan-B Cell Isolation Kit), blocked with streptavidin (Promega) and anti-human Fc receptor block (Invitrogen), then stained with 200ng of S-PE tetramers for 40 minutes at 4°C. Cells were subsequently stained for 20 minutes at 4°C with an Ab cocktail and labeled with barcoded TotalSeq-C Hashtag Abs 1-12 (BioLegend) (Supplemental Table 6) to facilitate downstream demultiplexing of samples. S-PE tetramer bound MBCs were sorted using a BD FACSymphony S6 SE analyzer (Figure 1, A-B). *Single-cell RNA-seq library preparation.* Sorted single-cells were encapsulated in droplets using the Chromium GEM-X Single Cell 5' Kit v3. 5' Cellular Indexing of Transcriptomes and Epitopes by Sequencing (CITE-Seq) gene expression libraries (10X Genomics, Single Cell 5' R2-only v3) and BCR V(D)J libraries (10X Genomics, Single Cell V(D)J R2-only v3) were prepared and sequenced on an Illmunia NovaSeq X Plus platform, with a target median sequencing depth of 50,000 read pairs per cell for gene expression libraries and 5,000 read pairs

609 per cell for BCR and CITE-Seq libraries. Two datasets were generated, one for each timepoint:
610 3-4 months post dose two or post dose three.
611 *Single-cell gene expression processing and data analysis*. FASTQ paired-end reads were
612 processed using 10x Genomics' Cell Ranger (v.8.0.0.0; "count" command) and aligned against
613 the human reference GRCh38-2024-A. The resulting filtered UMI count matrix generated from
614 the cellranger pipeline was loaded to generate Seurat objects (66). Cells were excluded from
615 analyses if the percentage of mitochondrial genes > 10%, number of unique features < 200, or
616 the number of unique features > 6500. Gene counts were normalized using Seurat's
617 NormalizeData function. TotalSeq-C hashtags were normalized by centered log-ratio (CLR)
618 normalization. Samples were demultiplexed using the HTODemux function and cell identities
619 were established based on the max HTO signal. Cells having a margin of less than 2.0 between
620 the max and secondary max HTO signal were excluded to prevent incorrect calling of the cell's
621 identity. Principle component analyses were performed using the top 2000 variable features
622 (regressing out isotype genes). Data from both timepoints were integrated using Harmony (67)
623 and dimensionality reduction was performed using uniform manifold approximation and
624 projection.
625 *Differential gene expression analysis*. Differentially expressed genes (DEGs) between clusters
626 were detected using the Seurat FindAllMarkers function and considered differentially expressed
627 if the adjusted P value < 0.05 and average $\log_2$(fold change) > 0.6. The FindMarkers function
628 was used to compare the same cluster between two study groups and DEGs were visualized on a
629 VolcanoPlot.
630 *BCR repertoire analysis.* V(D)J contigs were processed using the Immcantation framework
631 (v4.5.0) (68). Contigs were aligned to the IMGT reference using IgBLAST (v4.5.0) (68, 69).

Contigs containing non-productive sequences, missing a heavy chain or having multiple heavy chains, or lacking corresponding gene expression data were removed from analyses. Clonal analysis based on BCR heavy chain was conducted using SHazaM (68). The SCOPer hierarchialClones function was used to assign Ig sequences to clones, which utilizes a hierarchical clustering approach to define clones as groups of cells sharing common V and J gene annotations and CDR3 length (68, 70). Germline sequences were generated for each clone using Dowser and the IMGT reference database of known alleles (71, 72). SHazaM was used to calculate BCR SHM frequencies. Alakazam was used to perform diversity analyses and analyze Ig gene usage (68). Gene usage frequencies were compared to the CoV-AbDab public database of Abs and nanobodies able to bind coronaviruses (46), which we filtered to only include entries reporting human Ig genes and having specificity for SARS-CoV-2.

**Flow cytometry**

Cyro-preserved PBMCs were plated at 5 million cells per well, blocked with streptavidin and anti-human Fc receptor block (Invitrogen), then stained with 200ng of Wuhan SARS-CoV-2 S-PE tetramer per well for 40 minutes at 4°C. Cells were subsequently stained for 20 minutes at 4°C with a surface Ab cocktail (Supplemental Table 7) and acquired on a BD FACSymphony A3 cell analyzer.

**ELISA**

Plasma samples were diluted from 1:5 to 1:327,680 in 1% Blocker BLOTTO in PBST, for a total of 10 dilutions per sample. IgG and IgM Ab responses against the full-length Wuhan SARS-CoV-2 S trimer were measured using a chemiluminescent ELISA assay as previously described

(73). Effective concentration (EC50) values were calculated using the nlsLM function (74) and represent the plasma concentrations that give a response halfway between the assay's minimum value (blank controls) and a sample's maximum value. Details on data normalization and analysis are provided in the supplemental materials files, under methods.

**Anti-S IgG Avidity Assay**

High-binding plates (Sarstedt) were coated overnight at 4°C with 1μg/ml of trimeric Wuhan SARS-CoV-2 S protein, prepared as previously described (65). A positive control consisting of a pooled plasma mixture from eight SARS-CoV-2 mRNA vaccinated (three or more doses) healthy individuals, with or without natural infection, was used throughout. Plasma was heat-inactivated for 30 minutes at 56°C. Antigen-coated plates were blocked with blocking buffer (1X TBS + 0.1% Tween 20 + 2% BSA) at room temperature (RT). Patient plasma was serially diluted (3-fold, 7-point serial dilution from 1:100) with dilution buffer (1X TBS + 0.1% Tween 20 + 0.1% BSA) and 100μl was added to blocked plates in triplicates and incubated at RT for 1 hour. To assess avidity, 200μl of dilution buffer, 0.5M ammonium thiocyanate ($NH_4SCN$), 1M $NH_4SCN$, or 2M $NH_4SCN$ were added to appropriate wells, with a 15 minute incubation at RT. 100μl of horseradish peroxidase conjugated anti-human IgG, Fcγ specific (1:150,000 working dilution; Jackson ImmunoResearch) was then added to each well and incubated for 1 hour at RT. 100μl of HRP substrate (1-Step Ultra TMB-ELISA substrate solution; ThermoFisher) was added. After 10 minutes of development, 50μl of 2M sulfuric acid was added and optical densities were measured at 450nm. Avidity is reported as relative avidity index (%), fractional relative avidity index (%), and total relative avidity index (AU; avidity units). Calculations of avidity (Supplemental Table 5) were adapted from a previously reported assay (56).

## Statistics

Longitudinal multivariate regression analyses (STATA 18) of IgM and IgG levels controlled for age, sex, BMI, and vaccine type, with an interaction term between timepoint and study group. The aforementioned factors, with an additional term for IgG Ab concentration, were controlled for in analyses of IgG avidity. For non-longitudinal comparisons between study groups, where applicable, linear regressions (STATA 18) controlled for age, sex, BMI, and vaccine type or Kruskal-Wallis one-way ANOVA with Dunn's multiple comparisons tests (GraphPad Prism) were performed. Wilcoxon matched pairs signed rank two-tailed tests (GraphPad Prism) were performed to compare paired measurements across two timepoints. In all analyses, a P value of less than 0.05 was considered significant. Data represent mean ± 95% CI, unless otherwise noted.

## Study approval

This study was approved by the ethics boards of the University of Toronto (research ethics board [REB] protocol 27673), Mount Sinai Hospital/Sinai Health System (MSH REB 21-0022-E), and University Health Network–Toronto Western Hospital division (REB 21-5096). Written informed consent was obtained from all participants prior to participation.

## Data availability

Raw and processed CITE-Seq and BCR-Seq data can be found in NCBI GEO, under accession number GSE290006. Code used in this study are available in GitHub

(https://github.com/michelle-cheung25/Cheung_JCI2025). Values for all data points in graphs are reported in the Supporting Data Values file.

**Author Contributions:**

M.W.C, S.X, F.Q, M.D-B, K.C, R.M.D and T.H.W designed or conducted experiments, acquired and/or analyzed data. M.W.C prepared figures; M.W.C and T.H.W drafted the manuscript. J.S assisted with the recruitment of and processing of healthy donor blood for assay optimization, sample prep for single-cell RNA-Seq and provided guidance with statistical analyses. Y.L and J.R generated the Wuhan S proteins and S-PE tetramers for the following experiments: single-cell RNA-Seq, flow cytometry, avidity assays. J.D.L and J.M.S assisted with organizing and verifying patient metadata. V.C, M.S, A.-C.G, and T.H.W designed the IMPACT study and obtained research funding for the study. All authors edited and reviewed the manuscript.

**Acknowledgements:**

We thank Birinder Ghumman, Natalie Simard, and Gary Chao, for technical support, Troy Ketela and the Princess Margaret Genomics Centre for conducting single-cell RNA-Seq, and Alberto Martin and Goetz Ehrhardt for critical reading of the manuscript. We thank W. Rod Hardy for generating the variant-specific lentivirus constructs for the neutralization assay, with support from CoVaRR-Net, the Coronavirus Variants Rapid Response Network, funded by the Canadian Institutes for Health Research. The spike trimer, VHH72-Fc, and the anti-IgG-HRP for ELISA were kindly provided by The Pandemic Response Challenge Program of the National Research Council of Canada (Dr. Yves Durocher). We thank the Network Biology Collaborative Centre High-Throughput Screening Facility (RRID: SCR_025390) at the Lunenfeld-Tanenbaum Research Institute for assistance with the ELISA and neutralization assays. The facility is supported by the Canada Foundation for Innovation and the Ontario Government. This study was supported by a donation to the University of Toronto from Juan and Stefania Speck and by

Canadian Institutes of Health Research (CIHR)/COVID-Immunity Task Force (CITF) grant vs1-175545 (to A.-C.G), by CIHR grants FDN-143301 (to ACG) , FDN 143250 (to THW), GA2-177716 (V.C, A.-C.G, T.H.W), GA1-177703 (A.-C.G), by a CIHR Canada Graduate Scholarships Doctoral award FBD 187492 (M.W.C), by a Clinician Scientist Salary Award, Rheumatology, University of Toronto (to V.C), Canada Research Chair in Functional Proteomics (A.-C.G) and a Canada Research Chair in Anti-viral Immunity, University of Toronto (T.H.W).

**References:**


1. El-Gabalawy H, et al. Epidemiology of immune-mediated inflammatory diseases: incidence, prevalence, natural history, and comorbidities. *J Rheumatol Suppl.* 2010;85:2-10.
2. Collaborators GI. Global, regional, and national incidence of six major immune-mediated inflammatory diseases: findings from the global burden of disease study 2019. *EClinicalMedicine.* 2023;64:102193.
3. Monteleone G, et al. Immune-mediated inflammatory diseases: Common and different pathogenic and clinical features. *Autoimmunity Reviews.* 2023;22(10):103410.
4. Initiative GO-GaB. Top nine biological drugs by sales in 2023. https://gabionline.net/reports/top-nine-biological-drugs-by-sales-in-2023. Updated October 29 2024 Accessed January 24, 2025.
5. Baddley JW, et al. ESCMID Study Group for Infections in Compromised Hosts (ESGICH) Consensus Document on the safety of targeted and biological therapies: an infectious diseases perspective (Soluble immune effector molecules [I]: anti-tumor necrosis factor-alpha agents). *Clin Microbiol Infect.* 2018;24 Suppl 2:S10-S20.
6. Winthrop KL, et al. ESCMID Study Group for Infections in Compromised Hosts (ESGICH) Consensus Document on the safety of targeted and biological therapies: an infectious diseases perspective (Soluble immune effector molecules [II]: agents targeting interleukins, immunoglobulins and complement factors). *Clin Microbiol Infect.* 2018;24 Suppl 2:S21-s40.
7. Garcillan B, et al. Response to Vaccines in Patients with Immune-Mediated Inflammatory Diseases: A Narrative Review. *Vaccines (Basel).* 2022;10(2).

8. Cheung MW, et al. Third and Fourth Vaccine Doses Broaden and Prolong Immunity to SARS-CoV-2 in Adult Patients with Immune-Mediated Inflammatory Diseases. *J Immunol.* 2023;211(3):351-64.
9. Dayam RM, et al. Accelerated waning of immunity to SARS-CoV-2 mRNA vaccines in patients with immune-mediated inflammatory diseases. *JCI Insight.* 2022;7(11).
10. Lin S, et al. Antibody decay, T cell immunity and breakthrough infections following two SARS-CoV-2 vaccine doses in inflammatory bowel disease patients treated with infliximab and vedolizumab. *Nat Commun.* 2022;13(1):1379.
11. Geisen UM, et al. The long term vaccine-induced anti-SARS-CoV-2 immune response is impaired in quantity and quality under TNFalpha blockade. *J Med Virol.* 2022;94(12):5780-9.
12. Geisen UM, et al. Humoral protection to SARS-CoV2 declines faster in patients on TNF alpha blocking therapies. *RMD Open.* 2021;7(3).
13. Vollenberg R, et al. Humoral Immunity in Immunosuppressed IBD Patients after the Third SARS-CoV-2 Vaccination: A Comparison with Healthy Control Subjects. *Vaccines (Basel).* 2023;11(9).
14. Garner-Spitzer E, et al. Lower magnitude and faster waning of antibody responses to SARS-CoV-2 vaccination in anti-TNF-alpha-treated IBD patients are linked to lack of activation and expansion of cTfh1 cells and impaired B memory cell formation. *EBioMedicine.* 2023;96:104788.
15. Buhre JS, et al. Anti-TNF therapy impairs both short- and long-term IgG responses after repeated vaccination. *Allergy.* 2025;80(2):423-39.

16. Kobie JJ, et al. Decreased influenza-specific B cell responses in rheumatoid arthritis patients treated with anti-tumor necrosis factor. *Arthritis Res Ther.* 2011;13(6):R209.
17. Liu Z, et al. Antibody Responses to Influenza Vaccination are Diminished in Patients With Inflammatory Bowel Disease on Infliximab or Tofacitinib. *J Crohns Colitis.* 2024;18(4):560-9.
18. Gelinck LB, et al. The effect of anti-tumour necrosis factor alpha treatment on the antibody response to influenza vaccination. *Ann Rheum Dis.* 2008;67(5):713-6.
19. Salinas GF, et al. Anti-TNF treatment blocks the induction of T cell-dependent humoral responses. *Ann Rheum Dis.* 2013;72(6):1037-43.
20. Pasparakis M, et al. Immune and inflammatory responses in TNF alpha-deficient mice: a critical requirement for TNF alpha in the formation of primary B cell follicles, follicular dendritic cell networks and germinal centers, and in the maturation of the humoral immune response. *J Exp Med.* 1996;184(4):1397-411.
21. Matsumoto M, et al. Lymphotoxin-alpha-deficient and TNF receptor-I-deficient mice define developmental and functional characteristics of germinal centers. *Immunol Rev.* 1997;156:137-44.
22. Victora GD, Nussenzweig MC. Germinal Centers. *Annu Rev Immunol.* 2022;40:413-42.
23. Weisel FJ, et al. A Temporal Switch in the Germinal Center Determines Differential Output of Memory B and Plasma Cells. *Immunity.* 2016;44(1):116-30.
24. Endres R, et al. Mature follicular dendritic cell networks depend on expression of lymphotoxin beta receptor by radioresistant stromal cells and of lymphotoxin beta and tumor necrosis factor by B cells. *J Exp Med.* 1999;189(1):159-68.

25. Anolik JH, et al. Cutting edge: anti-tumor necrosis factor therapy in rheumatoid arthritis inhibits memory B lymphocytes via effects on lymphoid germinal centers and follicular dendritic cell networks. *J Immunol.* 2008;180(2):688-92.
26. Du SW, et al. Functional Characterization of CD11c(+) Age-Associated B Cells as Memory B Cells. *J Immunol.* 2019;203(11):2817-26.
27. Sanz I, et al. Challenges and Opportunities for Consistent Classification of Human B Cell and Plasma Cell Populations. *Front Immunol.* 2019;10:2458.
28. Palm A-KE, Kleinau S. Marginal zone B cells: From housekeeping function to autoimmunity? *Journal of Autoimmunity.* 2021;119:102627.
29. Descatoire M, et al. Identification of a human splenic marginal zone B cell precursor with NOTCH2-dependent differentiation properties. *Journal of Experimental Medicine.* 2014;211:987-1000.
30. Chakma CR, Good-Jacobson KL. Requirements of IL-4 during the Generation of B Cell Memory. *J Immunol.* 2023;210(12):1853-60.
31. Siu JHY, et al. Two subsets of human marginal zone B cells resolved by global analysis of lymphoid tissues and blood. *Sci Immunol.* 2022;7(69):eabm9060.
32. Al-Aubodah T-A, et al. The extrafollicular B cell response is a hallmark of childhood idiopathic nephrotic syndrome. *Nature Communications.* 2023;14(1):7682.
33. Elsner RA, Shlomchik MJ. Germinal Center and Extrafollicular B Cell Responses in Vaccination, Immunity, and Autoimmunity. *Immunity.* 2020;53(6):1136-50.
34. Gatto D, Brink R. B cell localization: regulation by EBI2 and its oxysterol ligand. *Trends Immunol.* 2013;34(7):336-41.

35. Barlev AN, et al. FcgammaRIIB regulates autoantibody responses by limiting marginal zone B cell activation. *J Clin Invest.* 2022;132(17).
36. Cox E-M, et al. AKT activity orchestrates marginal zone B cell development in mice and humans. *Cell Reports.* 2023;42(4).
37. Tangye SG, et al. Identification of functional human splenic memory B cells by expression of CD148 and CD27. *J Exp Med.* 1998;188(9):1691-703.
38. Gao X, Cockburn IA. The development and function of CD11c(+) atypical B cells - insights from single cell analysis. *Front Immunol.* 2022;13:979060.
39. Vastrad B, Vastrad C. Identification of differentially expressed genes and enriched pathways in inflammatory bowel disease using bioinformatics and next generation sequencing data analysis. *bioRxiv.* 2023:2023.06.01.543204.
40. Shi X, et al. Identification of a novel RPS26 nonsense mutation in a Chinese Diamond-Blackfan Anemia patient. *BMC Med Genet.* 2019;20(1):120.
41. Miller SA, et al. LSD1 and Aberrant DNA Methylation Mediate Persistence of Enteroendocrine Progenitors That Support BRAF-Mutant Colorectal Cancer. *Cancer Res.* 2021;81(14):3791-805.
42. Chung MKY, et al. Functions of double-negative B cells in autoimmune diseases, infections, and cancers. *EMBO Mol Med.* 2023;15(9):e17341.
43. Cerutti A, et al. Marginal zone B cells: virtues of innate-like antibody-producing lymphocytes. *Nat Rev Immunol.* 2013;13(2):118-32.
44. Karnell JL, et al. Role of CD11c(+) T-bet(+) B cells in human health and disease. *Cell Immunol.* 2017;321:40-5.

45. Hill MO. Diversity and Evenness: A Unifying Notation and Its Consequences. *Ecology.* 1973;54(2):427-32.

46. Raybould MIJ, et al. CoV-AbDab: the coronavirus antibody database. *Bioinformatics.* 2021;37(5):734-5.

47. Yaari G, et al. Models of somatic hypermutation targeting and substitution based on synonymous mutations from high-throughput immunoglobulin sequencing data. *Front Immunol.* 2013;4:358.

48. Perciani CT, et al. Improved method to calculate the antibody avidity index. *J Clin Lab Anal.* 2007;21(3):201-6.

49. Abu-Raya B, et al. Antibody and B-cell Immune Responses Against Bordetella Pertussis Following Infection and Immunization. *J Mol Biol.* 2023;435(24):168344.

50. Abu-Raya B, et al. The Effect of Timing of Tetanus-Diphtheria-Acellular Pertussis Vaccine Administration in Pregnancy on the Avidity of Pertussis Antibodies. *Front Immunol.* 2019;10:2423.

51. Correa VA, et al. Modified ELISA for antibody avidity evaluation: The need for standardization. *Biomed J.* 2021;44(4):433-8.

52. Semmes EC, et al. Understanding Early-Life Adaptive Immunity to Guide Interventions for Pediatric Health. *Front Immunol.* 2020;11:595297.

53. Ruel J, et al. IBD across the age spectrum—is it the same disease? *Nature Reviews Gastroenterology & Hepatology.* 2014;11(2):88-98.

54. Oyebanji OA, et al. Avidity maturation of humoral response following primary and booster doses of BNT162b2 mRNA vaccine among nursing home residents and healthcare workers. *Geroscience.* 2024;46(6):6183-94.

55. Pape KA, et al. Boosting corrects a memory B cell defect in SARS-CoV-2 mRNA-vaccinated patients with inflammatory bowel disease. *JCI Insight.* 2022;7(12).
56. Gaultier GN, et al. Adaptive immune responses to two-dose COVID-19 vaccine series in healthy Canadian adults >/= 50 years: a prospective, observational cohort study. *Sci Rep.* 2024;14(1):8926.
57. Roco JA, et al. Class-Switch Recombination Occurs Infrequently in Germinal Centers. *Immunity.* 2019;51(2):337-50 e7.
58. Turner JS, et al. SARS-CoV-2 mRNA vaccines induce persistent human germinal centre responses. *Nature.* 2021;596(7870):109-13.
59. Kim W, et al. Germinal centre-driven maturation of B cell response to mRNA vaccination. *Nature.* 2022;604(7904):141-5.
60. Ehling RA, et al. SARS-CoV-2 reactive and neutralizing antibodies discovered by single-cell sequencing of plasma cells and mammalian display. *Cell Rep.* 2022;38(3):110242.
61. Galson JD, et al. Deep Sequencing of B Cell Receptor Repertoires From COVID-19 Patients Reveals Strong Convergent Immune Signatures. *Front Immunol.* 2020;11:605170.
62. Scharf L, et al. Longitudinal single-cell analysis of SARS-CoV-2–reactive B cells uncovers persistence of early-formed, antigen-specific clones. *JCI Insight.* 2023;8(1).
63. Chen EC, et al. Convergent antibody responses to the SARS-CoV-2 spike protein in convalescent and vaccinated individuals. *Cell Rep.* 2021;36(8):109604.
64. Wang Y, et al. A large-scale systematic survey reveals recurring molecular features of public antibody responses to SARS-CoV-2. *Immunity.* 2022;55(6):1105-17 e4.

65. Abe KT, et al. A simple protein-based surrogate neutralization assay for SARS-CoV-2. *JCI Insight.* 2020;5(19).
66. Hao Y, et al. Dictionary learning for integrative, multimodal and scalable single-cell analysis. *Nat Biotechnol.* 2024;42(2):293-304.
67. Korsunsky I, et al. Fast, sensitive and accurate integration of single-cell data with Harmony. *Nat Methods.* 2019;16(12):1289-96.
68. Gupta NT, et al. Change-O: a toolkit for analyzing large-scale B cell immunoglobulin repertoire sequencing data. *Bioinformatics.* 2015;31(20):3356-8.
69. Ye J, et al. IgBLAST: an immunoglobulin variable domain sequence analysis tool. *Nucleic Acids Res.* 2013;41(Web Server issue):W34-40.
70. Gupta NT, et al. Hierarchical Clustering Can Identify B Cell Clones with High Confidence in Ig Repertoire Sequencing Data. *The Journal of Immunology.* 2017;198(6):2489-99.
71. Hoehn KB, et al. Phylogenetic analysis of migration, differentiation, and class switching in B cells. *PLoS Comput Biol.* 2022;18(4):e1009885.
72. Giudicelli V, et al. IMGT/GENE-DB: a comprehensive database for human and mouse immunoglobulin and T cell receptor genes. *Nucleic Acids Res.* 2005;33(Database issue):D256-61.
73. Colwill K, et al. A scalable serology solution for profiling humoral immune responses to SARS-CoV-2 infection and vaccination. *Clin Transl Immunology.* 2022;11(3):e1380.
74. Elzhov TV, et al. minpack.lm: R Interface to the Levenberg-Marquardt Nonlinear Least-Squares Algorithm Found in MINPACK, Plus Support for Bounds. Version 1.2-4. CRAN (2023). https://cran.r-project.org/web/packages/minpack.lm/index.html

## Figure and Figure Legends

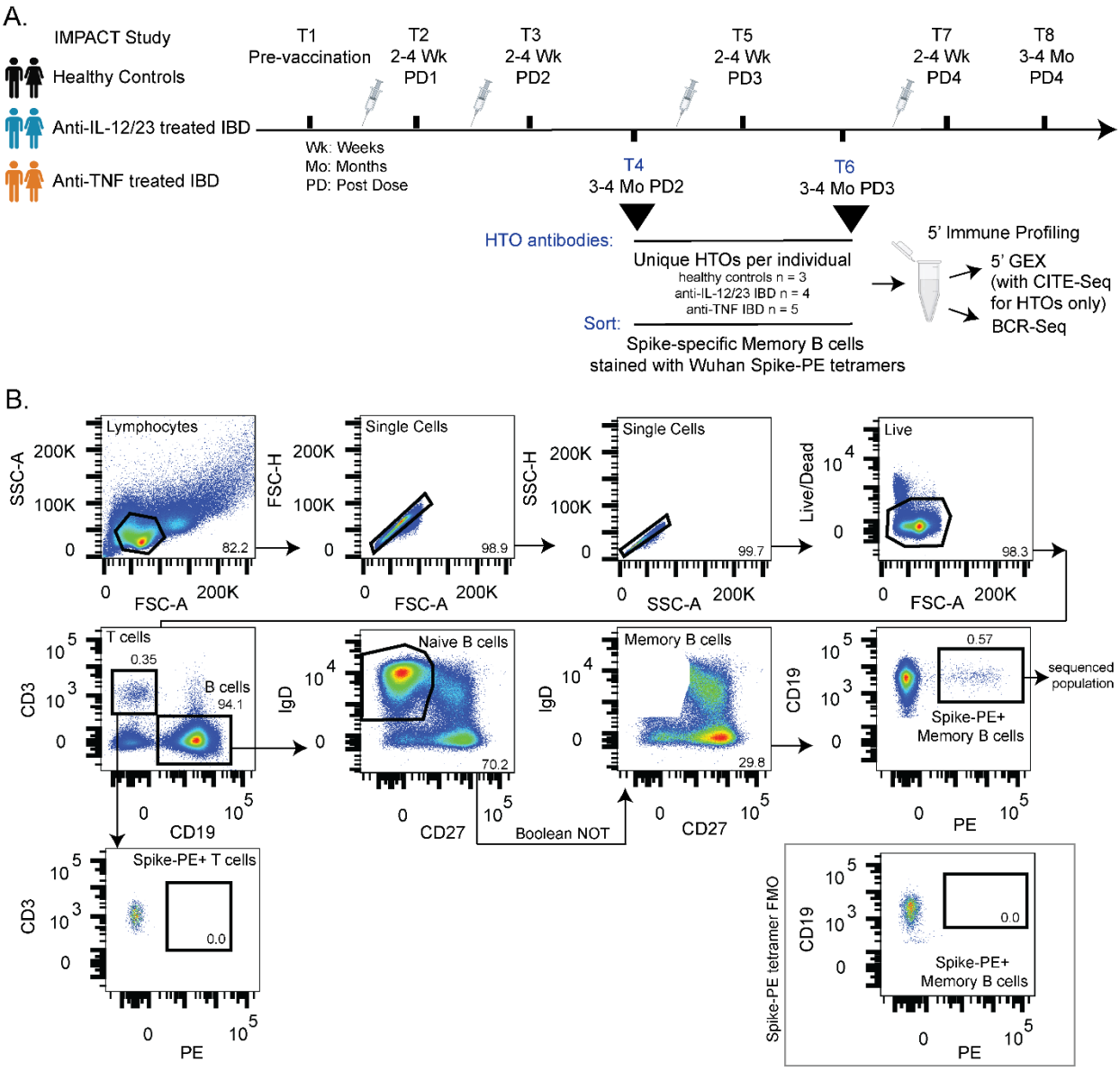


**Figure 1. Study design and isolation of S-specific memory B cells for single-cell RNA-Seq.**

**(A)** Study design. Blood was collected from healthy controls, anti-IL-12/23 treated inflammatory bowel disease (IBD) patients and anti-TNF treated IBD patients at timepoints (T) pre-vaccination and post one to four vaccine doses. From a subset of individuals (healthy controls, n=3; anti-IL-12/23 treated IBD patients, n =4; anti-TNF treated IBD patients, n = 5), B-cell enriched samples (following negative selection) from 3-4 months post dose 2 and post dose 3 were tagged with

unique TotalSeq-C Hashtag oligo-tagged (HTO) Abs and Wuhan SARS-CoV-2 S-specific (Spike-PE$^+$) memory B cells were sorted for single-cell RNA sequencing (5' gene expression with CITE-Seq for hashtags) and BCR-Seq. **(B)** Representative sorting strategy for S-PE tetramer bound (Spike-PE$^+$) memory B cells, gating on lymphocytes > singlets > live > CD19$^+$ B cells > memory B cells (not naïve B cells) > sorting for Spike-PE$^+$ memory B cells. The absence of non-specific binding of tetramer can be observed on CD3$^+$ T cells. A Spike-PE tetramer FMO sample is displayed in the grey box.

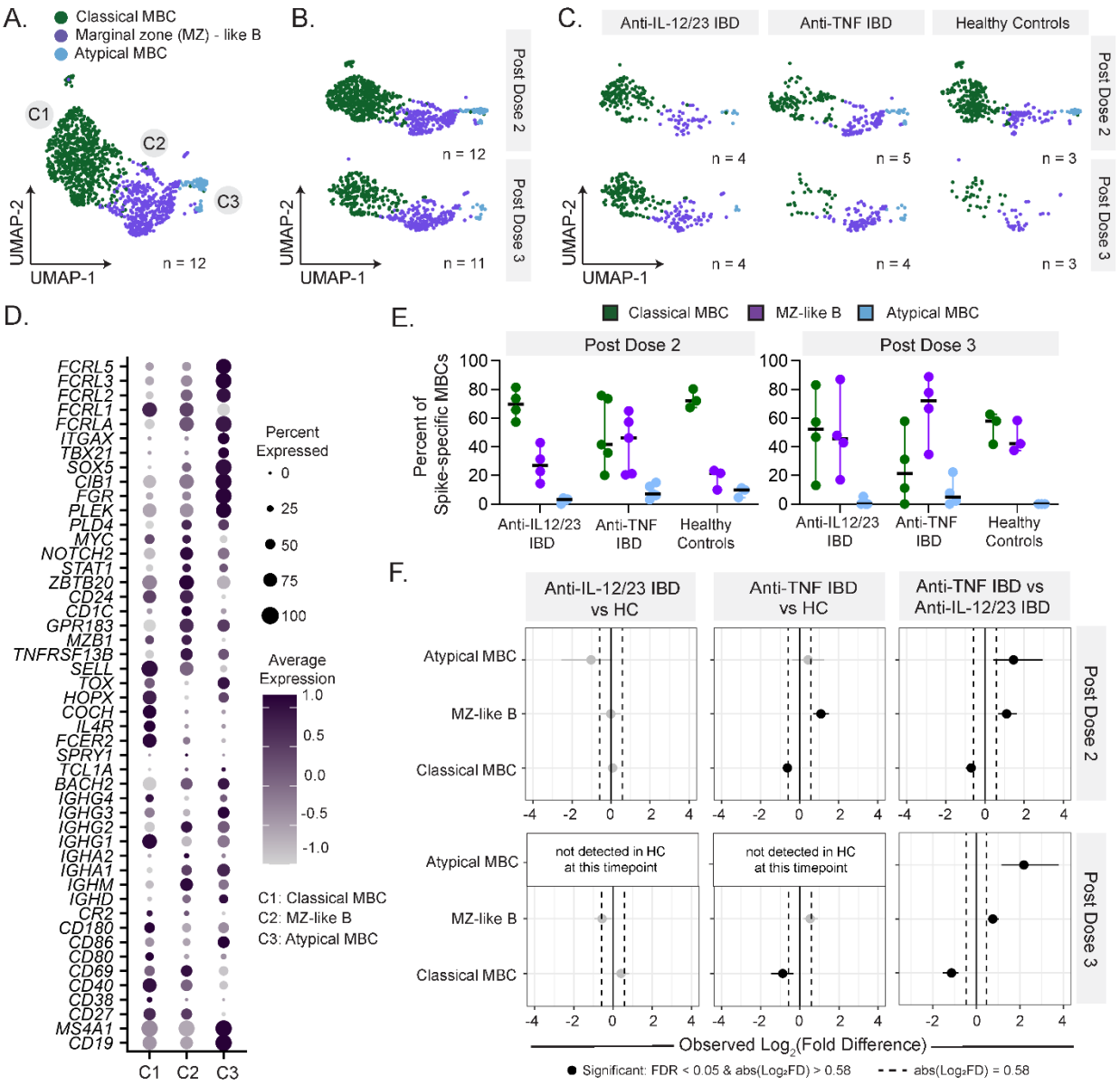


**Figure 2. Transcriptomic analysis reveals altered proportions of S-specific memory B cell subsets in anti-TNF treated IBD patients. (A)** Uniform manifold approximation and projection (UMAP) of S-specific memory B cells (MBC). Clusters are colored by subtype - C1: classical MBC, C2: marginal zone (MZ) – like B cells, C3: atypical MBC. Total number of individuals: n = 12 (healthy controls n = 3, anti-TNF treated IBD patients n = 5, anti-IL-12/23 treated IBD patients n = 4); total cell count: n = 1268. **(B)** UMAP of S-specific MBCs separated by

timepoint: 3-4 months post dose 2 (n cells = 824) or 3-4 months post dose 3 (n cells = 444). **(C)** UMAP of S-specific MBCs separated by timepoint and by study group: post dose 2 anti-IL-12/23 treated IBD (n cells = 215); post dose 3 anti-IL-12/23 treated IBD (n cells = 256); post dose 2 anti-TNF treated IBD (n cells = 252); post dose 3 anti-TNF treated IBD (n cells = 125); post dose 2 healthy controls (n cells = 357); post dose 3 healthy controls (n cells = 63). **(D)** DotPlot depicting the expression of selected genes. Dot size corresponds to the percentage of cells expressing the gene. Color intensity of the dots corresponds to the average expression across cells, where "0.0" represents the mean expression across the whole dataset. **(E)** Percentage of S-specific MBCs of each subset. Each dot represents one individual. Data represent median ± 95% CI. **(F)** Permutation tests were utilized to compare the proportion of S-specific MBCs classified as each MBC subset between study groups. The values colored in grey are non-significant; values colored in black are significant (false discovery rate (FDR) < 0.05 & absolute value of $\log_2$(fold difference) > 0.58. **(A-F)** Anti-IL-12/23 IBD: anti-IL-12/23 treated IBD patients; anti-TNF IBD: anti-TNF treated IBD patients.

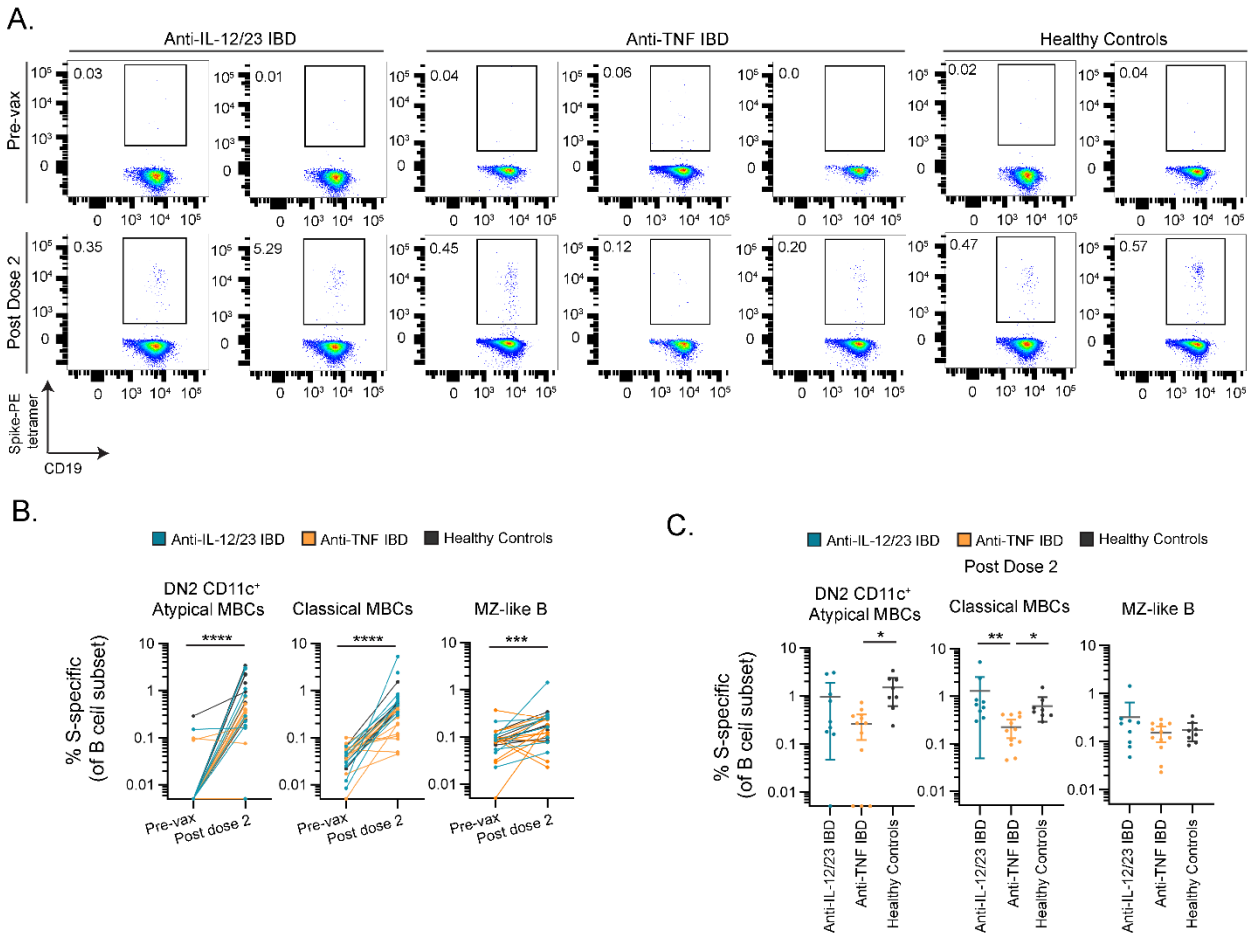


**Figure 3. Reduced S-specific classical memory B cells in anti-TNF treated IBD patients. (A)** Representative flow cytometric plots of S-specific classical memory B cells (MBC) from anti-TNF treated IBD patients (n=2), anti-IL-12/23 treated IBD patients (n=3) and healthy controls (n=3) at pre-vaccination and 3-4 months post dose 2. The frequency (%) of S-PE tetramer positive B cells is shown as a percentage of classical MBCs ($CD19^+$ $IgD^-CD27^+$). **(B)** Frequency of S-specific MBCs at pre-vaccination and 3-4 months post dose 2, grouped by MBC subset. Wilcoxon matched pairs signed rank two-tailed tests were performed. **(C)** Frequency of S-specific MBCs at 3-4 months post dose 2, grouped by MBC subset. Kruskal-Wallis one-way ANOVA with Dunn's multiple comparisons tests were performed. **(B-C)** Anti-IL-12/23 treated IBD patients (n = 9) are colored teal, anti-TNF treated IBD patients (n = 12) are colored orange,

and healthy controls (n = 8) are colored black. B cell subsets: DN2 (double negative) $CD11c^+$ atypical MBCs, classical MBCs and marginal zone (MZ) – like B cells. *P < 0.05; **P < 0.01; ***P <0.001; ****P <0.0001. Data represent mean ± 95% CI. Sample size information is provided in Supplemental Table 1. **(A-C)** Anti-IL-12/23 IBD: anti-IL-12/23 treated IBD patients; anti-TNF IBD: anti-TNF treated IBD patients.

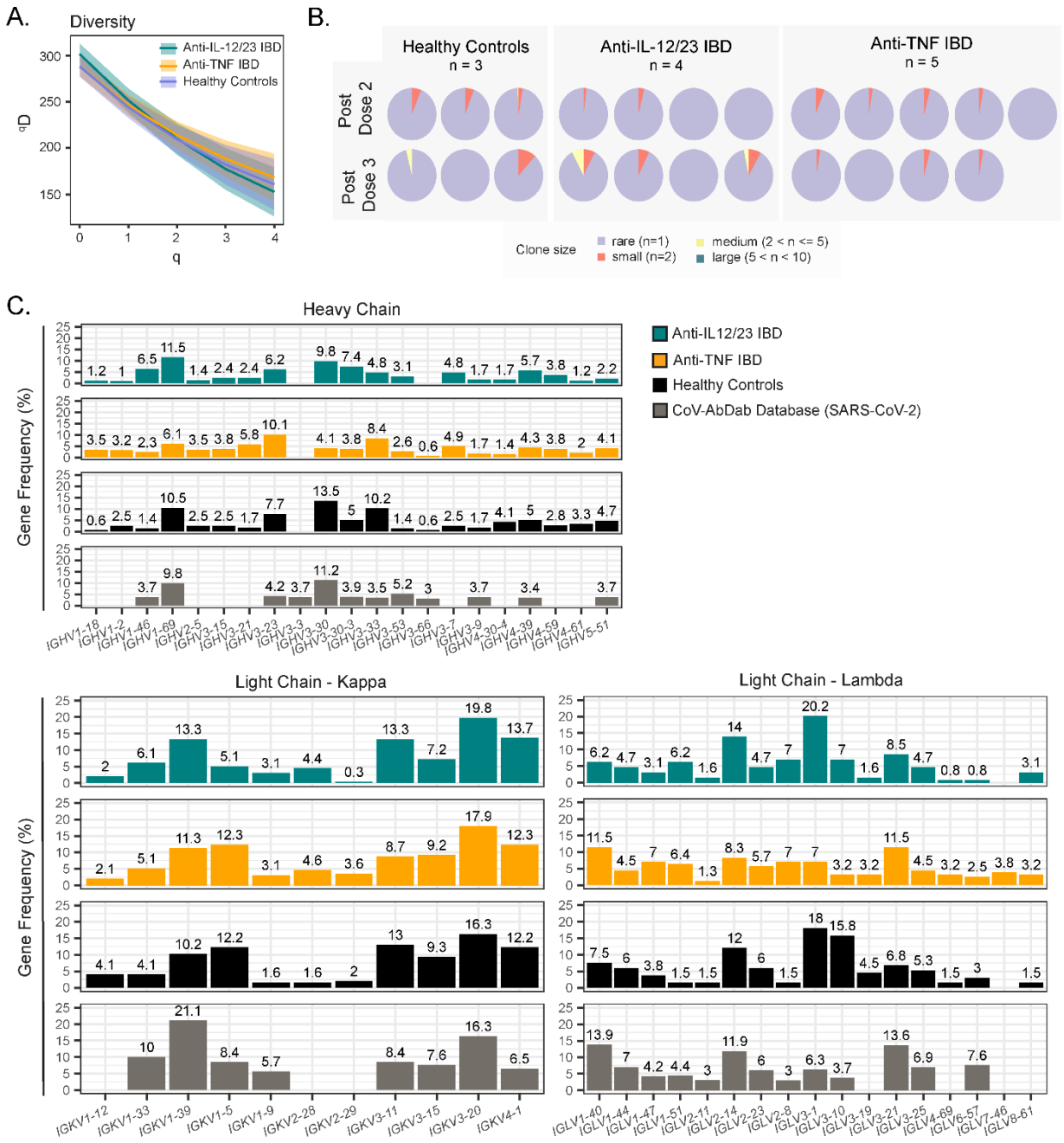


**Figure 4. Biased BCR heavy and light chain variable gene usage in S-specific memory B cells.** BCR-sequencing of healthy controls (n=3), anti-IL-12/23 treated IBD patients (n = 4), and anti-TNF treated IBD patients (n = 5), 3-4 months post dose 2 and 3. **(A)** Diversity (D) curve of S-specific MBCs grouped by study group (post dose 2 and dose 3 pooled). Diversity is calculated over a range of diversity orders, q (q=1 species richness; q = 2 Shannon entropy; q = 3 Simpson's

index). Shading represents confidence intervals. **(B)** Pie chart showing MBC clonal expansion indicated for each patient and timepoint. MBCs were binned into rare clones (n = 1 cell), small (n = 2 cells), medium (2 < n cells <= 5), or large (5 < n <= 10). **(C)** Frequency of heavy chain variable genes and light chain kappa and lambda variable genes in each study group compared to the CoV-AbDab database (filtered for SARS-CoV-2 specific entries). Only genes found in at least 3% of one of the four comparison groups are plotted.

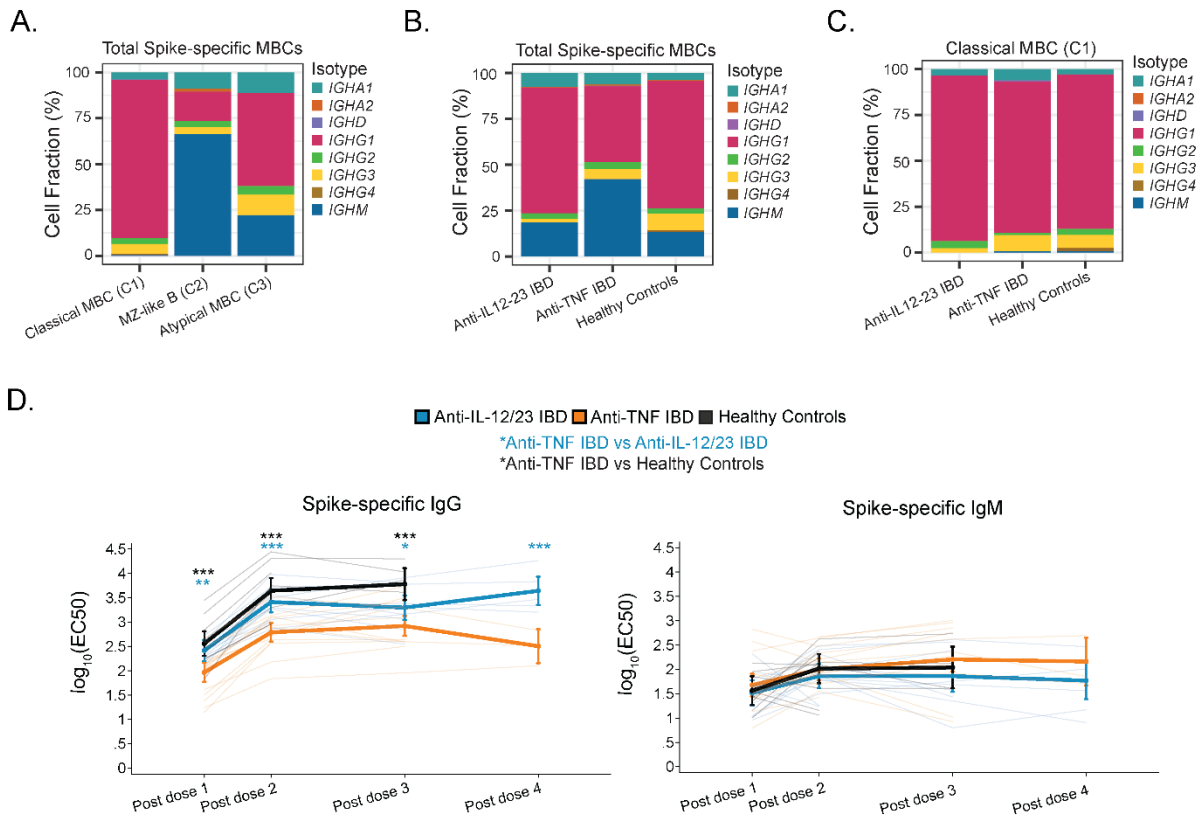


**Figure 5. Altered proportions of switched MBCs and plasma IgG in anti-TNF treated IBD patients. (A-C)** BCR-sequencing of S-specific MBCs 3-4 months post dose 2 and 3. **(A)** Fraction (%) of total S-specific MBCs (classical MBCs, marginal zone (MZ)-like B cells, and atypical MBCs) expressing each isotype. **(B)** Fraction (%) of total S-specific MBCs (classical MBCs, marginal zone (MZ)-like B cells, and atypical MBCs) expressing each isotype, grouped by study group. **(C)** Fraction (%) of S-specific classical MBCs (cluster 1) expressing each isotype, grouped by study group. **(D)** Level of plasma S-specific IgG and IgM across timepoints 2-4 weeks post one to four vaccine doses. EC50: sample dilution that gives a response halfway between the minimum signal of the assay and sample's own maximum (top) activity. *P < 0.05, **P < 0.01, ***P < 0.001, ****P < 0.0001. Asterisks in black indication comparisons between anti-TNF IBD group and healthy controls, asterisks in teal indication comparisons between anti-

TNF IBD group and anti-IL-12/23 IBD group. Thin lines represent each individual. Multivariate regression analyses controlled for age, sex, BMI, and vaccine type, with an interaction term between timepoint and study group. Data represent mean ± 95% CI. Sample size information is provided in Supplemental Table 2. **(A-D)** Anti-IL-12/23 IBD: anti-IL-12/23 treated IBD patients; anti-TNF IBD: anti-TNF treated IBD patients.

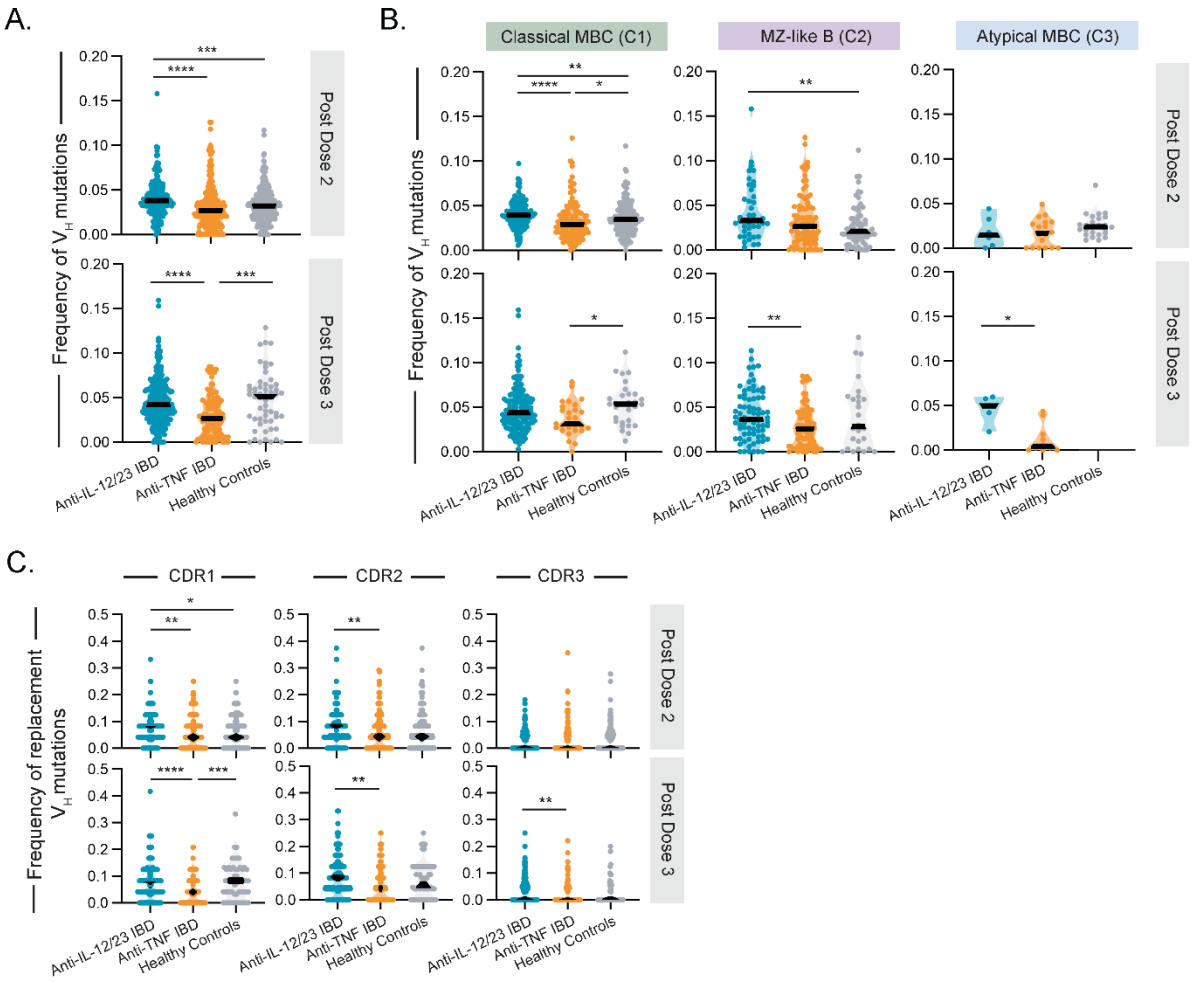


**Figure 6. Reduced somatic hypermutation in the BCRs of S-specific memory B cells in anti-TNF treated IBD patients.** BCR-Seq of S-specific memory B cells (MBCs) from healthy controls (n = 3), anti-IL-12/23 treated IBD patients (n = 4), and anti-TNF treated IBD patients (n = 5), post dose 2 and 3. Each dot represents a cell. **(A)** Frequency of somatic hypermutations (SHM) in the heavy chain variable region of S-specific MBCs (classical MBCs, MZ-like B cells, and atypical MBCs pooled), post dose 2 and post dose 3, grouped by study group. **(B)** Frequency of SHM in the heavy chain variable region of S-specific MBCs post dose 2 and 3, separated by subset (classical MBCs, marginal MZ-like B cells, atypical MBCs) and grouped by study group. **(C)** Frequency of replacement SHM in the heavy chain complementarity determining regions

(CDR) 1-3 of S-specific MBCs (classical MBCs, marginal zone (MZ)-like B cells, and atypical MBCs pooled), post dose 2 and 3, grouped by study group. **(A-C)** Frequency is calculated as counts of mutations over the total number of positions in the V gene sequence. Kruskal-Wallis one-way ANOVA with Dunn's multiple comparisons tests were performed. *P < 0.05, **P < 0.01, ***P < 0.001, ****P < 0.0001. Anti-IL-12/23 IBD: anti-IL-12/23 treated IBD patients; anti-TNF IBD: anti-TNF treated IBD patients.

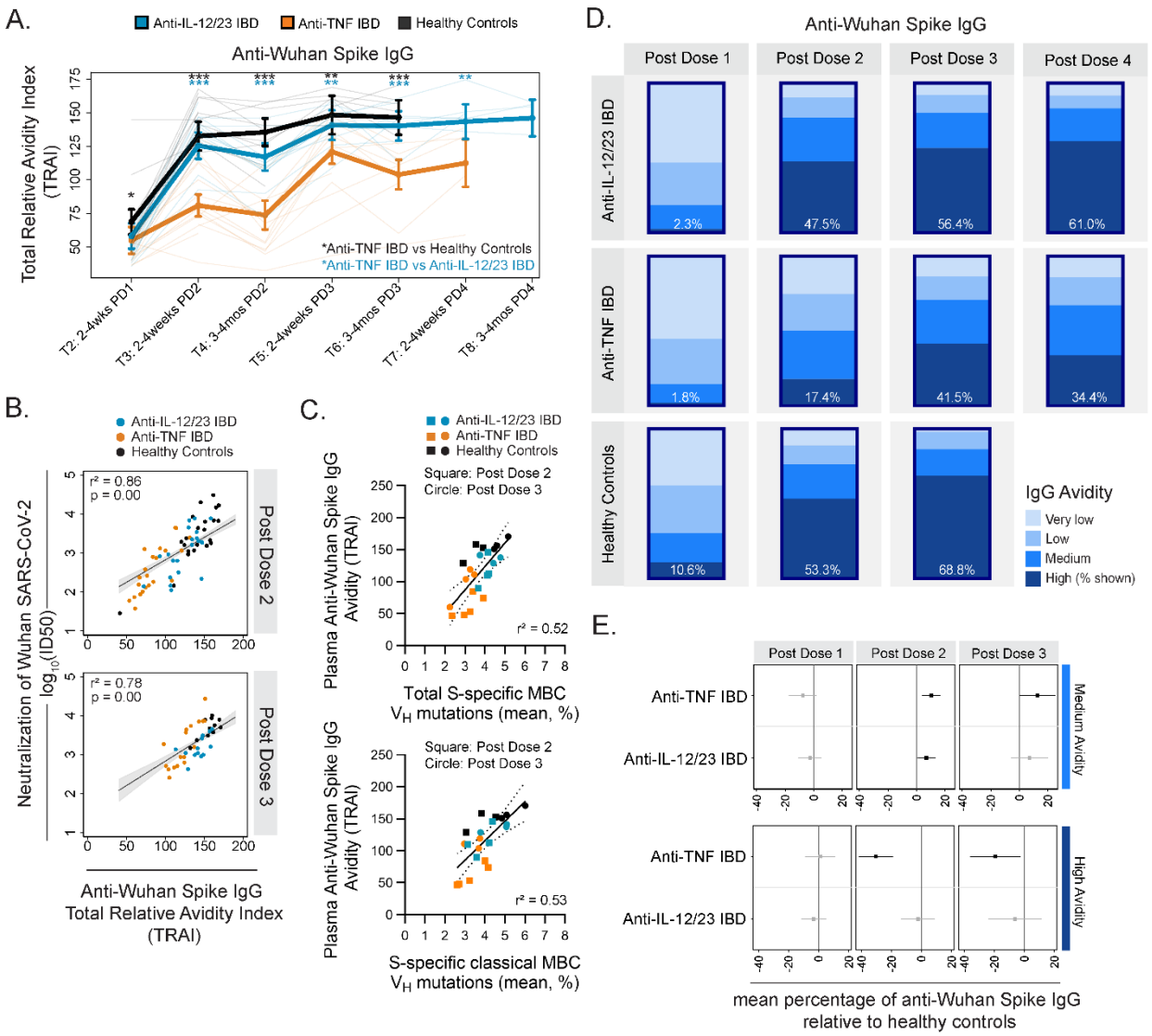


**Figure 7. Anti-TNF treated IBD patients have lower avidity anti-S IgG across four vaccine doses**. **(A)** Avidity (total relative avidity index, TRAI) of anti-Wuhan S IgG across one to four vaccine doses. Multivariate regression analyses controlled for age, BMI, sex, vaccine type, and IgG concentration, with an interaction term between timepoint and study group. Lines represent each individual. *P < 0.05, **P < 0.01, ***P < 0.001. Colored asterisks compare anti-TNF IBD patients with healthy controls (black) or with anti-IL-12/23 IBD patients (teal). **(B)** Association of anti-Wuhan S IgG avidity and neutralization of Wuhan SARS-CoV-2 post dose two and three.

Neutralization data were previously reported (8, 9). $Log_{10}$(ID50) – the serum dilution that inhibits 50% of lentiviral infection. Linear regressions controlled for age, BMI, sex, and vaccine type. **(C)** Association of mean frequency of heavy chain variable region somatic hypermutation in total S-specific memory B cells (MBCs) (classical MBCs, MZ-like B cells, atypical MBCs pooled) or S-specific classical MBCs and the avidity of anti-Wuhan S IgG. Linear regressions were performed. Each point represents an individual. **(D)** Mean percentage of anti-Wuhan S IgG that fall into each categorial avidity level: very low, low, medium, high. Percentage of high avidity IgG is denoted. Samples were obtained 2-4 weeks after each vaccine. Values are derived as fractional relative avidity indices (Supplemental Table 5). **(E)** Comparisons of the mean percentage of anti-Wuhan S IgG of each categorical avidity level in treated IBD patients relative to healthy controls, post one to three doses. Least squares regression controlled for age, sex, BMI, vaccine type and IgG concentration. Significant differences ($P < 0.05$) are colored black. **(A, D-E)** Sample size and timepoint information is provided in Supplemental Table 3. **(A, E)** Data represent mean ± 95% CI. **(A-E)** Anti-IL-12/23 IBD: anti-IL-12/23 treated IBD patients; anti-TNF IBD: anti-TNF treated IBD patients.

## Tables:

**Table 1.** Participant demographics: single-cell RNA sequencing

| Study Group | Healthy Controls Total, n = 3 | | | Anti-IL-12/23 IBD Total, n = 4 | | | | Anti-TNF IBD Total, n = 5 | | | | |
|---|---|---|---|---|---|---|---|---|---|---|---|---|
| **Donor ID** | **HC-01** | **HC-02** | **HC-03** | **IL12_23-01** | **IL12_23-02** | **IL12_23-03** | **IL12_23-04** | **TNF-01** | **TNF-02** | **TNF-03** | **TNF-04** | **TNF-05** |
| **Dose 1** | Pfizer | Pfizer | Pfizer | Pfizer | Pfizer | Pfizer | Pfizer | Pfizer | Pfizer | Pfizer | Moderna | Pfizer |
| **Dose 2** | Pfizer | Pfizer | Pfizer | Pfizer | Pfizer | Pfizer | Pfizer | Pfizer | Pfizer | Pfizer | Moderna | Pfizer |
| **Dose 3** | Pfizer | Pfizer | Pfizer | Pfizer | Pfizer | Pfizer | Pfizer | Pfizer | Pfizer | Moderna | Moderna | Pfizer |
| **Sex, M/F[A]** | F | F | F | F | M | F | F | M | F | F | M | M |
| **Timepoint: 3-4 MoPD2** | | | | | | | | | | | | |
| Age, y | 24 | 26 | 25 | 30 | 35 | 43 | 39 | 40 | 34 | 38 | 31 | 21 |
| Age of IBD diagnosis, y | N/A | N/A | N/A | 27 | 17 | 41 | 29 | 32 | 18 | 25 | 23 | 9 |
| BMI, kg/m$^2$ | 26.6 | 23.1 | 22.2 | 21.7 | 25.9 | 23 | 32.9 | 27.6 | 24.7 | 21.1 | 29.2 | 23.8 |
| Disease State | N/A | N/A | N/A | Remission | Remission | Remission | Remission | Remission | Remission | Remission | Remission | Remission |
| Infusion Medication[B] | None | None | None | Ustekinumab (90mg q8w) | Ustekinumab (90mg q4w) | Ustekinumab (90mg q8w) | Ustekinumab (90mg q4w) | Infliximab (600mg q6w) | Infliximab (500mg / kg) | Infliximab (300mg q4w) | Infliximab (700mg q8w) | Infliximab (600mg q6w) |
| **Timepoint: 3-4 MoPD3** | | | | | | | | | | | | |
| Age, y | 25 | 27 | 26 | 30 | 36 | 43 | 40 | 41 | 34 | 38 | 31 | N/A |
| Age of IBD diagnosis, y | N/A | N/A | N/A | 27 | 17 | 41 | 29 | 32 | 18 | 25 | 23 | N/A |
| BMI, kg/m$^2$ | 26.6 | 22.2 | 21.4 | 22.2 | 25.8 | 23 | 30.3 | 28.1 | 24.7 | 21.1 | 31.2 | N/A |
| Disease State | N/A | N/A | N/A | Remission | Remission | Remission | Remission | Remission | Remission | Remission | Remission | N/A |
| Infusion Medication[B] | None | None | None | Ustekinumab (90mg q8w) | Ustekinumab (90mg q4w) | Ustekinumab (90mg q8w) | Ustekinumab (90mg q4w) | Infliximab (600mg q6w) | Infliximab (500mg / kg) | Infliximab (300mg q4w) | Infliximab (700mg q8w) | N/A |

[A] M/F denotes male or female. [B] Type, dosage, and frequency (if known) of infusion medication. Abbreviations: BMI: Body Mass Index; IBD: Inflammatory bowel disease; IL: Interleukin; IQR: Inter-quartile range; kg: kilograms; m: meters; mg: milligrams; Mo: months; N/A: Not assessed, sample was not used; PD: Post dose; T: Timepoint; TNF: Tumor necrosis factor; q(#)w: every # weeks, y: years